

1

2 **A new multi-~~resolution-grid~~ bathymetric dataset of the Gulf of Naples (Italy) from** 3 **complementary multi-beam echosounders**

4

5 Federica Foglini¹, Marzia Rovere¹, Renato Tonielli¹, Giorgio Castellan^{1,2*}, Mariacristina Prampolini^{1,2},
6 Francesca Budillon¹, Marco Cuffaro³, Gabriella Di Martino¹, Valentina Grande¹, Sara Innangi¹, Maria
7 Filomena Loreto¹, Leonardo Langone⁴, Fantina Madricardo¹, Alessandra Mercorella¹, Paolo Montagna⁴,
8 Camilla Palmiotto¹, Claudio Pellegrini¹, Antonio Petrizzo¹, Lorenzo Petracchini³, Alessandro Remia¹,
9 Marco Sacchi¹, Daphnie Sanchez Galvez¹, Anna Nora Tassetti⁵, Fabio Trincardi⁶.

10

11 ¹ CNR –ISMAR - National Research Council, Institute of Marine Sciences, Italy;

12 ² NBFC - National Biodiversity Future Centre, Italy

13 ³ CNR-IGAG - National Research Council, Institute of Environmental Geology and Geoengineering, Italy;

14 ⁴ CNR ISP - National Research Council, Institute of Polar Sciences, Italy;

15 ⁵ CNR IRBIM- National Research Council, Institute for Biological Resources and Marine Biotechnologies, Italy;

16 ⁶ CNR-DSSSTA - National Research Council, Department of Earth Systems Science and Environmental Technologies, Italy.

17 *Correspondence to:* giorgio.castellan@cnr.it

18 **Abstract**

19 High-resolution bathymetry provides critical information to marine geoscientists. Bathymetric big data help characterise the
20 seafloor and its benthic habitats, understand sedimentary records, and support the development of offshore engineering
21 infrastructures. From September 27th to October 20th, 2022, the new CNR Research Vessel ~~GALA-BLU~~Gaia Blu explored the
22 seafloor of the Naples and Pozzuoli Gulfs, and the Amalfi coastal area (Tyrrhenian Sea, Italy) from 50 to more than 2000 m
23 water depth, acquiring about 5000 km² of multi beam echosounder data. This area is particularly vulnerable to abrupt changes
24 driven by the dynamics of several volcanic complexes, active in the area, and by human-induced impacts reflecting the
25 proximity to the highly populated and touristic coastal area of Naples and nearby famous islands. For these reasons, the seafloor
26 of the area needs to be known and constantly monitored. The digital bathymetric data previously available are restricted to the
27 shallow highly dynamic area of the Gulf of Naples and appear fragmented as they were acquired in successive years, with
28 different goals thereby using a variety of devices, with markedly different spatial resolutions. In this paper, we present
29 bathymetric maps of the Gulf of Naples and adjacent slope basins at unprecedented resolution using three state-of-the-art multi
30 beam echosounders. These high-resolution data highlight the technological advances of geophysical surveys achieved over the
31 last 20 years and contribute to assessing the most dynamic areas where changes in the seafloor over time can be quantified.
32 The new digital multi-resolution bathymetric products are openly accessible via Marine Geosciences Data System MGDS

ha formattato: Apice

33 (refer to section Data Availability, Table 8, for datasets and products DOIs), perfectly matching the FAIR (Findable,
34 Accessible, Interoperable and Reusable) and Open Science Principles.

35 1. Introduction

36 In 2018, GEBCO and the Nippon Foundation joined forces to establish the Nippon Foundation GEBCO Seabed 2030 Project
37 (Mayer et al., 2018), an international effort to foster the complete mapping of the world ocean by 2030. Despite many years
38 of mapping efforts unveiled increasingly larger portions of the seabed, only about 25% of the world oceans seafloor is mapped
39 to date at high resolution (<https://seabed2030.org/our-mission/>). Obtaining a high-resolution map of the world's seafloor is
40 crucial to understanding how oceans work, from geodynamics and geohazards aspects, to the interactions between seafloor
41 morphology and bottom-current dynamics, and to the distribution and ecological status of benthic habitats [to cite a few](#)
42 [applications](#). In the last 40 years, almost two-thirds of marine environments have been “severely altered” by human activity
43 (Díaz et al., 2019) resulting in significant biodiversity loss and erosion of the ecological services and goods (Worm et al.,
44 2006). In this context, the European Union has implemented a governance framework specifically aiming at assessing,
45 monitoring, and preserving the status of the marine benthic natural heritage (Marine Strategy Framework Directive MSFD,
46 2014/89/EU), but also at promoting the sustainable exploitation of marine and coastal resources (European MSP Directive,
47 2008/56/EC). Among the European Seas, the Mediterranean Sea is a hotspot of biodiversity, hosting more than 7.5% of global
48 biodiversity (Bianchi and Morri, 2000) with a high percentage of endemic species (Myers et al., 2000) and unique ecosystems.
49 However, the basin is recognized to be “under siege” due to the historical and still ongoing impacts from multiple stressors
50 such as littering and dumping, trawling, ghost fishing, seaborne traffic and modification of the seafloor (Coll et al., 2012; Puig
51 et al., 2012; Madricardo et al., 2017, 2019; Canals et al., 2021; Budillon et al., 2022; Pellegrini et al., 2023; Trincardi et al.,
52 2023). This is particularly evident in the Gulf of Naples, a densely populated coastal region stretching along 385 km on the
53 eastern Tyrrhenian Sea, which represents an important tourist destination including the Gulf Islands (Capri, Ischia and
54 Procida), Sorrento Peninsula, Vesuvius National Park, Phlegraean Fields and archaeological sites of Pompeii, Herculaneum,
55 Pozzuoli and Cuma.

56 The underwater landscape of the Gulf of Naples is geomorphologically complex, with large canyon systems, marine landslides,
57 debris flow deposits, volcanic apparatuses; the area includes various benthic habitats of ecological relevance from the shore to
58 the deep sea, such as *Posidonia oceanica* meadows (e.g., MATTM, 2004), animal forests (e.g., Bavestrello et al., 2014), cold-
59 water corals (CWC, Taviani et al., 2019; Angiolillo et al., 2023), and hydrothermal vent communities (e.g. Apolloni et al.,
60 2020; Donnarumma et al., 2019). The gulf region also hosts numerous archaeological and cultural heritage sites, threatened
61 by natural and human pressures (Mattei et al. 2019). To preserve marine biodiversity and the historical value of the area, four
62 Marine Protected Areas (MPAs) have been established: the Underwater Parks of Baia and Gaiola MPAs, the Regno di Nettuno
63 MPA and the Punta Campanella MPA (Apolloni et al., 2018).

64 The first extensive high-resolution mapping of the seafloor of the gulf was performed in the framework of the Italian geological
65 mapping research program (1997-2017); through bathymetric surveys of the continental shelf/slope system of the Campania
66 region, using numerous multi beam echosounder systems (MBESs) with an ~~average~~ vertical resolution of < 0.25% of the water
67 depth and position accuracy better than 10 m. The data, acquired at different resolutions, were merged to create a Digital
68 Terrain Model (DTM) with a homogeneous grid and with a cell spacing of 20 m (Aiello et al., 2020). This map highlighted
69 the most prominent geomorphological features in the coastal zone such as the canyons, banks, debris avalanches, hydrothermal
70 vents and volcanoclastic basement outcrops with high ecological value habitats in urgent need of preservation (Taviani et al
71 2019). This valuable dataset was shared in gridded form, within the EMODnet project, as 1/16 arc minutes (ca. 115 m) DTMs.
72 High-resolution data for selected areas are also available as 1/128 or 1/256 arc minutes (ca.15 m or 7 m) HR-DTMs
73 (<https://emodnet.ec.europa.eu/geoviewer/>).
74 Despite the significant effort of ongoing national and international projects and infrastructures worldwide to make data
75 available, such as GEBCO (<https://www.gebco.net>) and EMODnet (<https://emodnet.ec.europa.eu/en>), local high-resolution
76 datasets and raw data are typically not yet accessible (Sievers et al., 2021). Indeed, ~~databases~~ local datasets are often generated,
77 hosted, and administered by various institutes in the world with dissimilar data policies, which often do not follow the Findable,
78 Accessible, Interoperable and Reusable (FAIR) data principles (Stall et al., 2019).

79 This study presents the results of a high-resolution geophysical survey named JammeGaia22 conducted in October 2022 on
80 board R/V Gaia Blu using three different state-of-the-art MBESs (Kongsberg EM 2040, EM 712, and EM 304) and aims at
81 improving the knowledge of the seascape of the Gulf of Naples by enhancing the analysis/visualization of seabed morphology
82 through high-resolution digital bathymetric models.

~~83 Given the unprecedented high- and multi-resolution survey conducted in the study area and the availability of ancillary data
84 such as backscatter and water column data, this dataset represents a unique benchmark for future studies related to geohazards
85 assessment, sediment transport, fishery management, resource exploration and sustainable exploitation, maritime spatial
86 planning and decision-making, marine ecosystem and habitat mapping, oceanographic modeling including storm surges and
87 scenarios of tsunami wave propagation.~~

~~88 We discuss the quality of the data collection (section Data Quality) and present three examples that highlight the potential
89 applications of this dataset (Section Results and discussion). Our contribution also aims at highlighting the innovative approach
90 used during JammeGaia22 (Section Multibeam data processing), where data are processed daily on board and can be made
91 available to the scientific community and the generic public in near-real-very short time via a geoportal, making the datasets
92 FAIR and facilitating interdisciplinary research within the Open Science Principles. We describe the bathymetric and
93 backscatter datasets in detail highlighting its potential applications (Section Results and discussion) thanks to the good quality~~

Formattato: SpazioDopo: 12 pt

94 of the data collection discussed in the section Data Quality. Finally, we provide full access to the whole dataset, the bathymetric
95 grids and backscatter mosaics produced, and the metadata as explicated in section Data availability.

96 Given the unprecedented high- and multi-resolution survey conducted in the study area and the availability of ancillary data
97 such as backscatter and water-column data, this dataset represents a unique benchmark for future studies related to geohazards
98 assessment, sediment transport, fishery management, resource exploration and sustainable exploitation, maritime spatial
99 planning and decision making, marine ecosystem and habitat mapping, oceanographic modeling including storm surges and
100 scenarios of tsunami wave propagation.

101 We discuss the quality of the data collection (section Data Quality) and present three examples that highlight the potential
102 applications of this dataset (Section Results and discussion).

103

104 **2 Study area - Geological and geomorphological background**

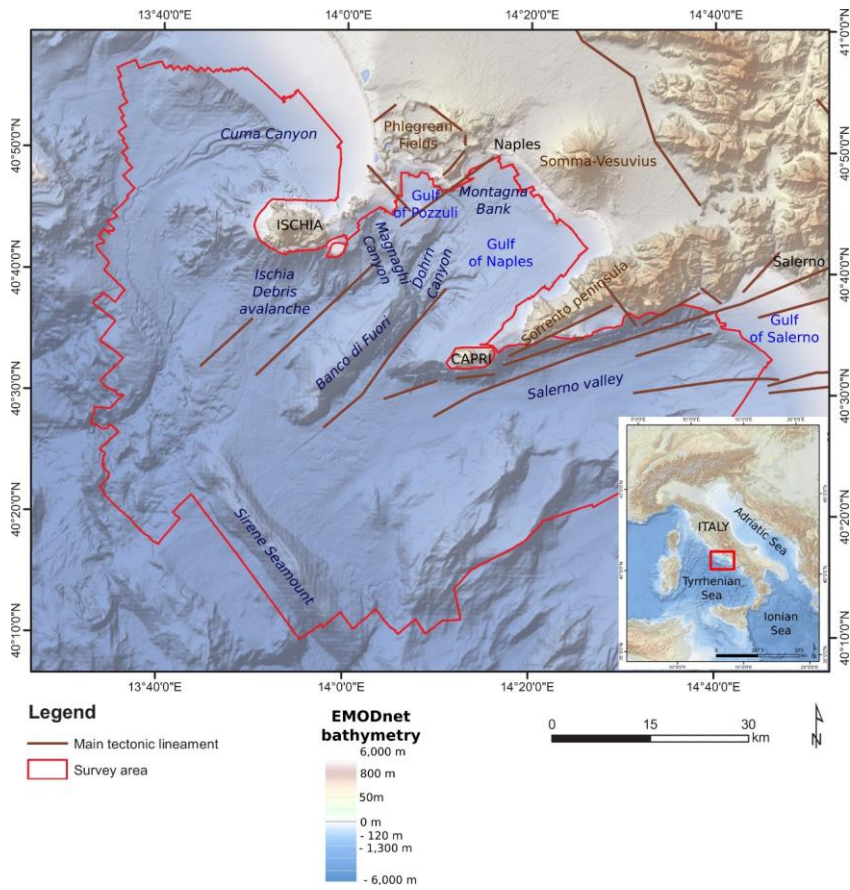
105 The investigated area belongs to the central-eastern margin of the Tyrrhenian Sea, encompassing the region between the
106 western margin of the Southern Apennines thrust belt and the Tyrrhenian abyssal plain (ca.3000 m deep; Figure 1). The
107 Tyrrhenian Sea is the youngest back-arc basin of the Mediterranean Sea that developed since the Middle Miocene (Trincardi
108 and Zitellini, 1987; Kastens et al., 1988; Lymer et al., 2018; Loreto et al., 2021; Miramontes et al., 2023) reflecting the east-
109 and south-eastward retreat of the Ionian slab, guided by the Africa-Europe convergence (Moussat et al., 1985; Malinverno and
110 Ryan, 1986; Kastens et al., 1988). The Campania segment of the eastern Tyrrhenian margin is characterized by a series of NE-
111 SW trending half-graben bounded by structural highs that have developed since the early Pleistocene and accommodate the
112 tectonic-controlled subsidence of the alluvial plains along with their submerged counterparts, namely the Gaeta Gulf, the Gulf
113 of Naples and the Gulf of Salerno (Figure 1; Romano et al., 1984; Ruberti et al., 2022; Amato et al., 2011; Bellucci et al.,
114 2006).

115 Structural lineaments also control the preferential pathways of volcanic activity, particularly in the last 2 My. Volcanic activity
116 followed an eastward migration, governing the geomorphological setting of the region and promoting deposition of
117 sedimentary sequences up to 3 km thick (Milia, 1999; Milia et al., 2003). The Phlegraean Fields volcanic area is a 78-ka old
118 active poly-calderic system (Scarpati et al., 2012) that has affected its territory in the last millennia and has strongly influenced
119 the evolution of the adjacent coasts during the late Pleistocene and Holocene, which has been mainly shaped by three super-
120 eruptions. The oldest one was the Campanian Ignimbrite (CI) eruption that occurred at ca. 35-40 ka BP (Giaccio et al., 2017).
121 After this main event, the northern part of the just-formed caldera was submerged by the sea. The second eruption, which led
122 to the formation of the Masseria Del Monte Tuff, occurred at 29.3 ka BP (Albert et al., 2019). The Neapolitan Yellow Tuff
123 (NYT; Deino et al. 2004) eruption at ca. 15 ka BP contributed to the formation of the youngest caldera (Orsi et al., 1992),
124 nowadays well documented also offshore (Sacchi et al., 2014; Steinmann et al., 2016, 2018). Besides volcanic eruptions,

125 alternating long-term magma/hydrothermal fluid inflation and deflation processes controlled the morphological evolution of
126 this area. Further, short-term vertical, meter-scale, ground movements characterised times immediately preceding and
127 following each eruption, which produced rapid relative sea-level variations along the entire coastal sector (Isaia et al., 2019
128 and reference therein). The area has experienced high rates of subsidence (approx. 4.0 mm/yr) through the Pleistocene
129 (Torrente et al., 2010; Milia et al., 2017; Iannace et al., 2018), accompanied by the activity of major NE–SW-striking faults.
130 At present, intense seismicity, including the Md 4.0 earthquake occurred on 2nd October 2023, is instead associated to the
131 18.0 mm/yr uplift of the central portion of the Phlegraean Field area.

132 Volcanic activity, long-term vertical ground movements, glacio-eustasy and the rapid dismantling of the emerging landscapes
133 have driven a rapid geomorphological evolution of the margin, resulting in steep slopes, canyoning, deep-sea fan accretion and
134 gravitational slope instability. Extensive lateral collapses of the volcanic edifices have been documented offshore, south of
135 Ischia Island (Chiocci et al., 1998; Chiocci and de Alteriis, 2006; de Alteriis et al., 2010), possibly occurred also in historical
136 time, and two others of minor extent to the west and north of Ischia Island (Budillon et al., 2003; Violante et al., 2003) and in
137 the Gulf of Naples (Milia et al., 2008, 2012; Passaro et al., 2018). The rapid aggradation of volcanoclastic deposits in shallow
138 marine environment and the entrance of pyroclastic flows into the seawater also led to seafloor instability and creep in the
139 prodelta offshore the main rivers (Sacchi et al., 2005; 2009).

140 Three main turbiditic systems, namely Cuma, Magnaghi and Dohrn Canyons, and the deep structurally controlled Salerno
141 Valley, have developed along with the rising of intra-slope reliefs and volcanic activity, and acted as main conduits delivering
142 sediment towards deeper-water domains (Passaro et al., 2016). These features characterize the present-day seafloor
143 morphology and, although partially inactive, are of paramount interest as hotspots of biodiversity in the Mediterranean Sea
144 (e.g., Taviani et al., 2019; Mussi et al., 2022).



145

146 Figure 1. Map of the study area in the central Tyrrhenian Sea showing the main physiographic and tectonic features (modified from Aiello
 147 et al., 2020). Elevation and bathymetry from EMODnet bathymetry (<https://emodnet.ec.europa.eu/en/bathymetry>).

148

149 **3. Materials and methods**

150 **3.1 Multi beam data acquisition**

151 Multi beam data were collected during the JammeGaia22 cruise from September 27th to October 20th 2022 using three different
152 MBES: the Kongsberg EM2040-04 MKII 0.4°x0.7° suited for water depths between 50 and 150 m, Kongsberg EM712 1°x0.5°
153 for water depths between 150 and 1000 m and Kongsberg EM304 MKII 1°x1° for water depth greater than 1000 m (Table
154 1 for acquisition settings).

155 Table 1. Acquisition settings for the three multi beam echosounder systems.

MBES	Water depth (m)	Frequency (kHz)	Angular coverage (degree)	Ping rate (Hz)	Acquisition mode
EM2040	50-100	300	65	1.5	Deep
EM2040	100-150	200	70	1.5	Very deep
EM712	150-600	70-100	70	2	Shallow
EM712	600-1000	40-100	70	2	Deep
EM304	>1000	30	65	>5	Auto

156
157 The MBESs were hull-mounted on the R/V ~~GAIA-BLU~~Gaia Blu gondola with a T-configuration of linear transducer arrays.
158 A Seapath 380 system was used for ship positioning, supplied by a Fugro HP differential Global Positioning System (DGPS),
159 with Marinestar GNSS signal accuracy better than 5 cm. The Kongsberg motion sensor MRU (Motion Reference Unit) 5 and
160 a Dual Antenna GPS integrated into the Seapath, were used to correct for pitch, roll, heave and yaw movements (reaching
161 0.02° roll and pitch accuracy, and 0.075° heading accuracy). A Valeport mini SVS sensor was positioned close to the
162 transducers to ~~e~~continuously measure the sound velocity for the beamforming. ~~This sound velocity (SV) value was continuously~~
163 ~~compared to that from Sound velocity profiles (SVP) in use to warn when a new profile was required. However, the difference~~
164 ~~between SV from the SVS sensor and in-use profile never reached warning values. Sound velocity profiles (SV, since SVPPs)~~
165 were systematically collected at least twice a day with a Valeport Midas SVP, for a total of 40 SVPs. Data were logged,
166 displayed and checked in real-time by the Kongsberg data acquisition and control software SIS 5 (Seafloor Information
167 System). A ~~software~~ tool ~~included in SIS 5 software~~ was used to extend the SVPs down to 12000 m water depth. Since the
168 Mediterranean Sea is characterized by a stratified water column with peculiar changes in the physical-chemical properties
169 (Tanhua et al. 2013; Rossi et al. 2014; Basterretxea et al. 2018), a linear regression based on the collected SVP data was run
170 in R software (R Core Team, 2019) to estimate the sound velocity values down to 12000 m depth.

171
172 Professional topographers measured the offsets of the instruments with millimetric accuracy using a dedicated dimensional
173 survey of the ship's hull at dry dock.

174 Sensors have been calibrated during the Sea Acceptance Tests (roll, pitch, time and heading offsets) and were also regularly
175 checked in post-processing (Table 2 for calibration values).

176 Table 2. Calibration values applied after the Sea Acceptance Test.

MBES	Pitch	Roll	Heading
EM2040	+0.10°	+0.5°	-0.20°
EM304	00.00°	+0.2°	0.00°
EM712	-0.10°	-0.07°	-0.15°

177

178 We kept a 20% overlap between lines to ensure 100% of bathymetric coverage, avoiding the influence of external beams of
179 bad quality given by possible residual errors in roll, ~~and~~ sound speed profile measurements and poor seafloor detection. The
180 multi beam operated with an average swath opening angle of about 65°/70° (Table 1) for each multi beam system. The vessel
181 sailed with a reasonably constant speed of 8 knots, considered ideal to have the minimum noise and tested during the Sea
182 Acceptance Test. Sea conditions were good and stable for the entire survey, with wave height almost always lower than 1 m.
183 Seafloor and water column backscatter data were collected simultaneously during bathymetric data acquisition.

184

185 3.2 Multibeam data processing

186 The bathymetric data collected every day were ~~immediately~~ processed on-board during nightshift on-board to produce DTMs
187 and backscatter mosaics, which were then uploaded daily the next morning in a dedicated WebGIS to inform the scientific
188 community on the progress of the campaign and make the data openly available. The data processing workflow is summarized
189 in Figure 2.

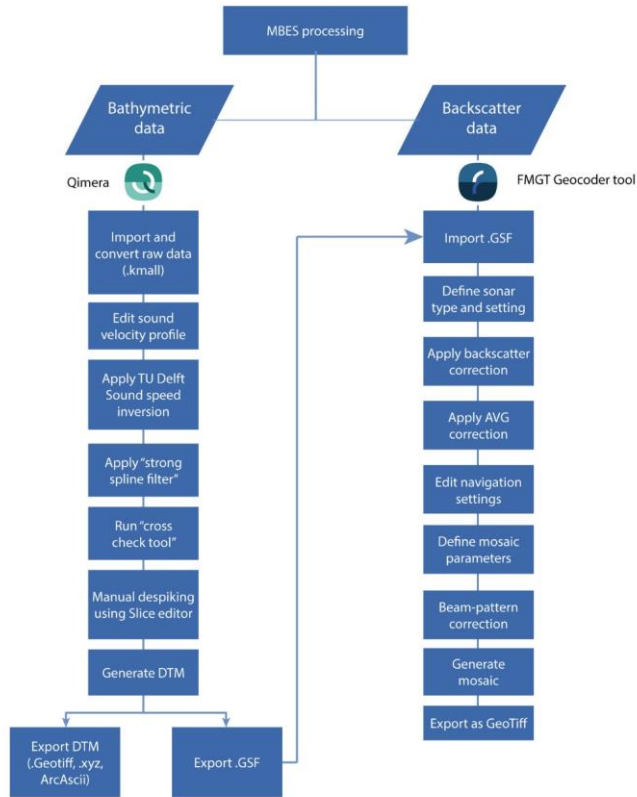


Figure 2. Workflow of bathymetric and backscatter data processing, [described in 3.2.1 and 3.2.2-](#)

190
191
192

193 3.2.1 Bathymetric data processing

194 The processing of the raw data was carried out using the QPS Qimera v.2.5.0 software (Quality Positioning Services BV, Zeist,
195 Netherlands) following a standard procedure, which includes sound speed correction, removal of erroneous soundings, and
196 correction of vertical offsets [from a previous swath](#). The quality of the data was initially checked using the 'Cross Check Tool'
197 to check for soundings with significant offsets from the local mean water depth.

198 When sound velocity errors were evident in the data, the TU Delft Sound Speed Inversion tool (Beaudoin et al., 2018) was
 199 used to correct the profile. The tool applies an algorithm that allows a completely automated refraction error correction. It
 200 works by taking advantage of the overlap between survey lines to simultaneously estimate sound speed correction for a given
 201 set of pings and their neighbours, by computing a best-fit solution that minimizes the mismatch in the areas of overlap between
 202 lines (Mohammadloo et al., 2019). The settings applied for TU Delft Sound Inversion were data-specific, depending on the
 203 quality of the SVP, upon initial assessment. ~~Nevertheless, we typically applied the ‘Quick Search’ algorithm and ‘Coarse’~~
 204 ~~configuration as an initial setting, and we then applied adjustments if necessary~~
 205
 206 After the sound speed correction, the strong spline filter of Qimera allowed removal of soundings beyond the local mean water
 207 depth (offsets); the remaining offsets (if any) were removed manually using the ‘Slice editor’ of Qimera. The processed
 208 bathymetric data were exported into GSF format for backscatter processing and to a gridded surface data (GeoTIFF). The
 209 resolution of the GeoTIFF was defined based on the water depth and the footprint calculated for each sonar used (Table 3).

211 Table 3. Calculated footprints of ensonified seafloor area at different water depths for each MBES, relative grid resolution chosen and
 212 mean of the number of soundings in each grid cell. Products and dataset are available at section Data Availability.

MBES	Water Depth (m)	TX Footprint (m)	RX Footprint (m)	Insonified area (mm²)	Grid resolution (m)	<u>Number of soundings per grid cell</u>
EM2040 (0.4°x 0.7°)	50	0.4363	0.6109	0.92	2	<u>7.12</u>
	60	0.5236	0.7330	1.10		
	70	0.6109	0.8552	1.28		
	80	0.6981	0.9774	1.46		
	90	0.7854	1.0996	1.65		
	100	0.8727	1.2217	1.83		
EM712 (0.5°X1°)	150	1.3090	2.6181	3.28	5	<u>23.87</u>
	200	1.7453	3.4907	4.37	10	<u>17.35</u>
	300	2.6180	5.2361	6.56		
	400	3.4907	6.9815	8.75		
	500	4.3634	8.7269	10.94	15	<u>9.96</u>
	600	5.2360	10.4722	13.12		
	700	6.1087	12.2176	15.31		
	800	6.9814	13.9630	17.50		
					20	

Tabella formattata
 ha formattato: Non Evidenziato
 ha formattato: Apice , Non Evidenziato
 ha formattato: Non Evidenziato
 ha formattato: Inglese (Stati Uniti)

	900	7.8540	15.7084	19.69		<u>13.9</u>
	1000	8.7267	17.4537	21.87		
EM304 (1°X1°)	1000	17.4537	17.4537	30.94	30	<u>21.72</u>
	1100	19.1991	19.1991	34.03		
	1200	20.9445	20.9445	37.12		
	1300	22.6899	22.6899	40.22	40	<u>25.45</u>
	1400	24.4352	24.4352	43.31		
	1500	26.1806	26.1806	46.40		
	1600	27.9260	27.9260	49.50		
	1700	29.6714	29.6714	52.59		
	1800	31.4167	31.4167	55.68		
	1900	33.1621	33.1621	58.78		
	2000	34.9075	34.9075	61.87		

213

214

215 3.2.2 Backscatter data post-processing

216 The MBES backscatter data were processed using the QPS Fledermaus Geocoder Tool (FMGT) v.7.10.2 software. The
 217 processed MBES data (.gsf) were used to apply backscatter corrections, beam pattern correction, and angle-varying gain
 218 (AVG) corrections to the backscatter data. After these corrections, FMGT applied the sonar's navigation data (i.e., XY
 219 coordinates, roll, heading, pitch, heave) to ~~georeference the backscatter value~~~~improve the spatial accuracy of the data~~. The
 220 DTM generated in Qimera provided a ~~reference bathymetric~~ grid to improve backscatter corrections. The reference grid was
 221 included by the FMGT software to determine topographic slope, while the corrected bathymetry in the source files (i.e., GSF)
 222 was regularly used to geo-reference the snippet trace from a single ping to the correct ~~spot position~~ on the seafloor ~~and with~~
 223 ~~the correct scaling~~ (Quality Positioning Services B.V., 2020). Finally, the backscatter snippets were mosaicked with the 'No
 224 Nadir possible, 25% overlap' algorithm to reduce the banding effect, and 30-40% line blending was applied to blend the pixels
 225 in the overlapping areas. The mosaics were gridded in various resolutions (Table 4) with dB values cropped to $\pm 3\sigma$ and
 226 logarithmically mapped to 8-bit scale. These mosaics were exported as 'One merged Colored GeoTIFF format'.

227

228 Table 4. Resolution of backscatter mosaic for each MBES. Products and dataset are available at section Data Availability.

MBES	Mosaic resolution (m)
EM2040	5 m

EM712	10 m
EM304	30 m

229

230 3.3 Bathymetric derivatives

231 A geomorphometric analysis of the seabed was carried out using ArcGIS to emphasize any subtle variation in seafloor
 232 morphology. The geomorphometric indices calculated were slope, broad-scale and fine-scale Bathymetric Position Index
 233 (BPI), and ~~rugosity~~ vector ruggedness measure.

234 The slope is a first-order derivative of the bathymetry and represents seabed maximum inclination (in any direction) in degrees,
 235 the slope was measured in ArcGIS as the maximum rate of change in value from a cell to its immediate neighbours. The
 236 calculation is performed using the average maximum technique (Burrough and McDonnell, 1998). using the AreaSlope
 237 algorithm, included in Marine Toolbox for ESRI ArcGIS developed by Dr Tim Le Bas (Le Bas 2016), picking an area of 3x3
 238 pixels around each cell. Values are real numbers between 0.0° and 90.0°, areas of no data have a conventional value of -1.0.
 239 Depth values in input were smoothed before calculation of the slope using a user-defined smoothing window of 3x3. This
 240 approach served to removed local changes giving a regional value for slope and diminishing edge effect (Dolan, 2012).

241 Broad- and fine-scale BPIs were calculated using Benthic Terrain Modeler (BTM) toolbox for ArcGIS (Walbridge et al., 2018;
 242 Lundblad et al., 2006). ~~BPI is derived from an input bathymetric data set BPI is a second-order derivative (as it is derived from~~
 243 ~~the slope) of the bathymetry and is modified a modification~~ from topographic position index as defined by Weiss (2001) and
 244 Iampietro and Kvitek (2002). It evaluates differences in elevation between a focal point and the mean elevation of the
 245 surrounding cells within a user-defined window. Values range from -1 to +1, with negative values reflecting depressions in
 246 the seabed, null values for planar areas and positive values denoting ~~the positive~~ reliefs. Broad-scale BPI allows the
 247 identification of main regional features within the seafloor, while fine-scale BPI helps identify smaller features of the benthic
 248 landscape. The values used to calculate BPIs for all the bathymetric surfaces are reported in Table 5.

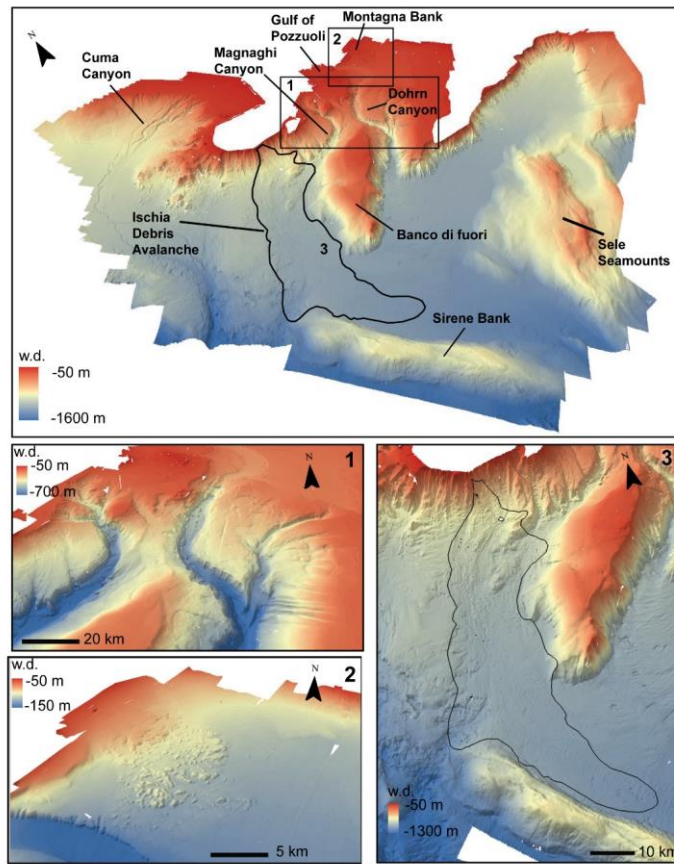
249 Vector ruggedness measure (VRM) quantifies terrain ruggedness by measuring the dispersion of vectors orthogonal to the
 250 terrain surface (Sappington et al., 2007). VRM shows low values both in flat and steep areas, but high values in areas that are
 251 both steep and rugged.

252 4. Results and Discussion

253 4.1 Multi-resolution-grid bathymetric grid-dataset

254 The ~~multi-resolution-grid~~ bathymetric dataset covers an area of about 5000 km² offshore the Gulf of Naples from 50 to more
 255 than 2000 m water depth (Figure 3). The different resolutions, depending on the water depth and the MBES footprint, of the

256 acquired data reveal the complexity of the seafloor with unprecedented details and allow to better discriminate
257 geomorphological features already described in the literature (D'Argenio et al., 2004).
258
259



260
261 Figure 3. Bathymetric map of the study area (20 m resolution, 2 vertical exaggeration) showing the main seabed features; (1) multibeam
262 bathymetry (20 m resolution, x2 vertical exaggeration) of the Dohrn and Magnaghi canyon systems; (2) multibeam bathymetry of the
263 Montagna Bank area; and (3) multibeam bathymetry of the debris avalanche offshore the Ischia Island.

264 Coupled with other indices, this high-resolution bathymetry not only is valuable information to study sediment dynamics, and
 265 morphotectonics of canyons, structural highs and seamounts, but also represents a baseline to investigate the presence and
 266 distribution of benthic habitats and infer hydrological transients ~~hugging at~~ the sea floor. To demonstrate how the newly
 267 acquired data allow to appreciate the variations of the seafloor, broad- and fine-scale BPI were calculated from the bathymetry
 268 in three selected sectors of the study area using the parameters reported in Table 5.

269

270

Table 5. Inner and outer radius used for calculation of Bathymetric Position Index (BPI) for selected areas by depth range.

Area	Depth range (m)	Resolution (m)	Broad-scale BPI Inner – outer radius (cells)	Fine-scale BPI Inner – outer radius (cells)
Canyons of the Gulf of Naples	50-100	2	30-60	2-5
	101-200	5	12-30	2-5
	201-500	10	6-15	2-5
	501-700	15	4-9	2-5
	701-1000	20	3-8	2-5
	1001-2500	30	2-5	2-5
Montagna Bank	50-100	2	30-60	5-8
	101-200	5	12-30	5-8
	201-500	10	6-15	5-8
Ischia debris avalanche	50-100	2	30-60	1-3
	101-200	5	12-30	1-3
	201-500	10	6-15	1-3
	501-700	15	4-9	1-3
	701-1000	20	3-8	1-3
	1001-1900	30	2-5	1-3

271

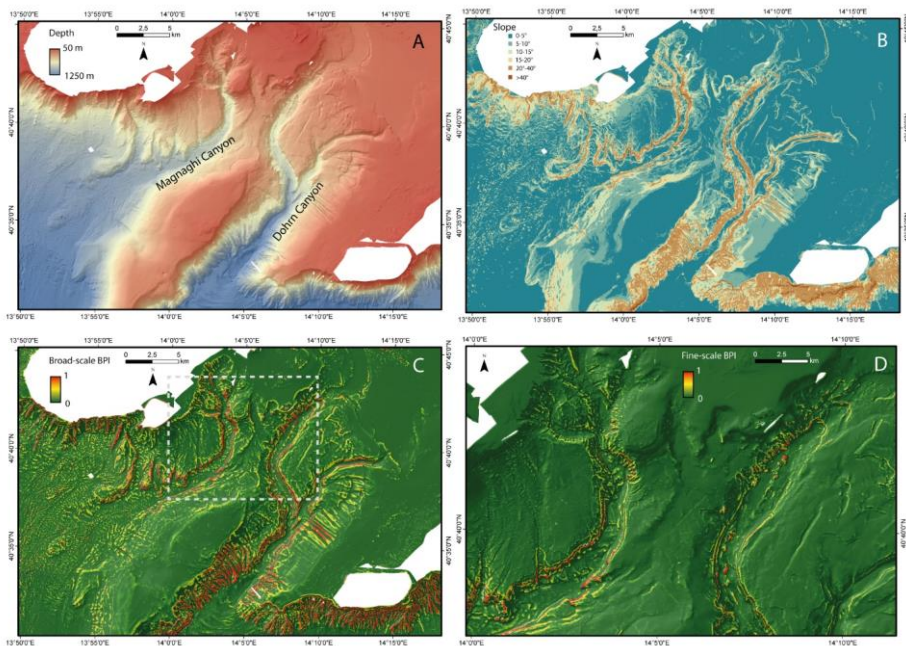
272 4.1.1 Canyons of the Gulf of Naples

273 The morphology of the Dohrn and Magnaghi Canyons is possibly controlled by the presence of extensional faults coupled
 274 with the volcanic activity characterising the area. Both canyons acted as large drainage systems within this proximal marine
 275 area during the Late Quaternary (Aiello et al., 2020 and references therein). The two branches of Dohrn Canyon are about 500
 276 m wide and show a V-shaped profile in the upper part and a U-shaped profile in the lower part, suggesting uniform sediment
 277 fill of the thalweg. The bathymetric derivatives confirm the complexity of these drainage patterns, ~~showing some differences~~
 278 ~~possibly~~ related to the stratigraphy of the eroded terrains and to the recurrence and or competence of the flows flushing the

ha formattato: Non Evidenziato

279 two systems: straight gullies characterise the flanks of Dohrn Canyon and normally do not indent the outer shelf, with the
280 exception of the area NW of Capri (Fig. 4). Canyon Dohrn emanates from Ammontatura channel, on the inner shelf, a possibly
281 active sediment conduit also during sea level rise and high stand conditions; Dohrn Canyon undercuts its secondary branch
282 located north of Capri Island under-excavating its base by 50m. The straight gullies on the flanks of Dohrn Canyon are hanging
283 above the canyon thalweg suggesting the activity of powerful flows along the axis of the canyon. Moreover, the fine-scale BPI
284 highlights terrace rims along Dohrn Canyon flanks and slide scars with a slide deposit at their foot (Aiello et al., 2020), as well
285 as the gullies with head scarps and along-slope small-scale sand splays located on the southern flank of Banco di Fuori. Dohrn
286 Canyon shows a radial bedform field in its lower portion where the canyon broadens, and its floor decreases its gradient.
287 Comparison with pre-existing data in this area suggests that the bedform field has not moved in the last two decades.
288 In contrast, Magnaghi Canyon is shorter, less deeply incised and not gullied on its flanks, possibly reflecting its lack of
289 connection to a major source of sediment-laden flows. The right-hand side of the canyon shows short and straight incisions
290 with marked bedforms that appear reminiscent of cyclic steps (Kostic, 2011; Slootman and Cartigny, 2020) and can be clearly
291 discerned on the slope map and on the ~~DPI-BPI~~ maps.

292



293

294

295

296

Figure 4 (A) Bathymetric data of canyons of the Gulf of Naples; (B) Slope; (C) positive values of broad-scale and (D) fine-scale BPI of a portion of the area (dashed rectangle in C) calculated from the newly acquired multi-resolution grid, showing the drainage pattern of the Dohrn and Magnaghi canyons.

297

4.1.2 Cuma Channel

298

Cuma Channel is a complex sediment conduit characterized by 1) an upper section, between the shelf-edge and the base of Gaeta basin, where three independent sub parallel channels present gullied heads, low sinuosity and flat channel floor; 2) a relatively narrow thalweg characterized by a prominent high sinuosity on the sub-horizontal floor of Gaeta Basin and 3) a straighter channel, proceeding in deeper waters across the steepening slope region.

300

301

302

Peering-Pairing both bathymetric and backscatter images prompt several questions that will be worth addressing in future cruises, after collecting complementary core and seismic-stratigraphy data. In particular:

303

304

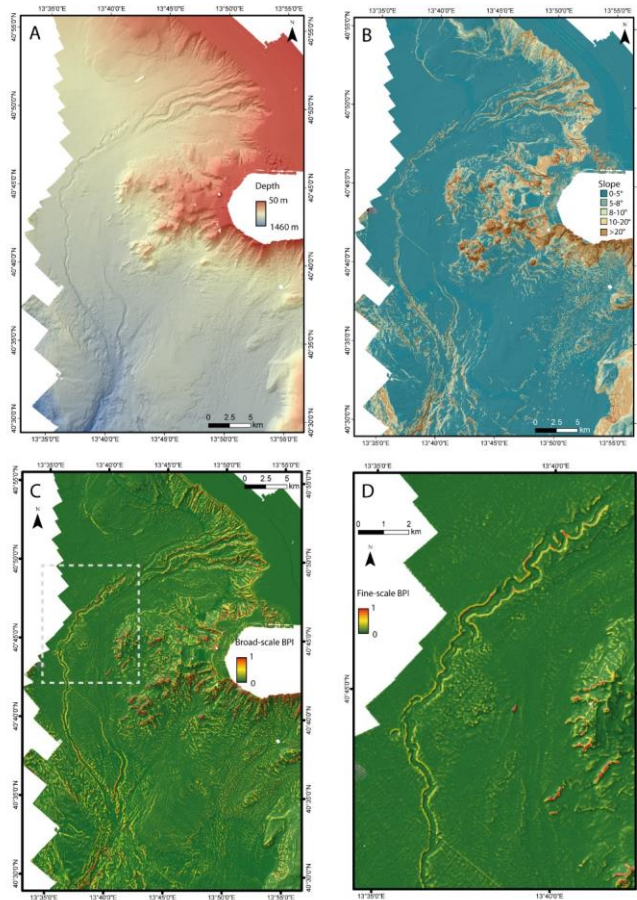
305

306

307

- 1) there is no continuity between either of the three channels dissecting the upper slope and the high sinuosity channel on the floor of Gaeta basin; however, backscatter images hint to a seaward continuity of the most meridional of the three slope channels characterized by higher backscatter and, likely, coarser grained sediment. This channel reaches a north-south orientation before widening and rapidly reducing its seafloor reflectivity;

308 2) the high sinuosity to the west is therefore disconnected from its original feeder, upslope, and, proceeding downslope,
309 bends gently to the Southeast and then to the Southwest in the lowermost tip of the mapped area; interestingly, the
310 region located west of this gentle, multi-kilometric, bend is carved by several barchan-like scours that can be
311 hypothetically ascribed to overflows of a much larger volume compared to the size of the channel conduit;
312 3) knowing that the Volturno prodelta has reached the shelf edge, it is possible that hyperpycnal flows from the river
313 ignite flows on the slope that are capable to hug the seafloor and reshape its morphology, as documented during the
314 modern sea level high stand in some other example of high discharge systems like the Crati River (Lucchi et al.,
315 1983).
316



317

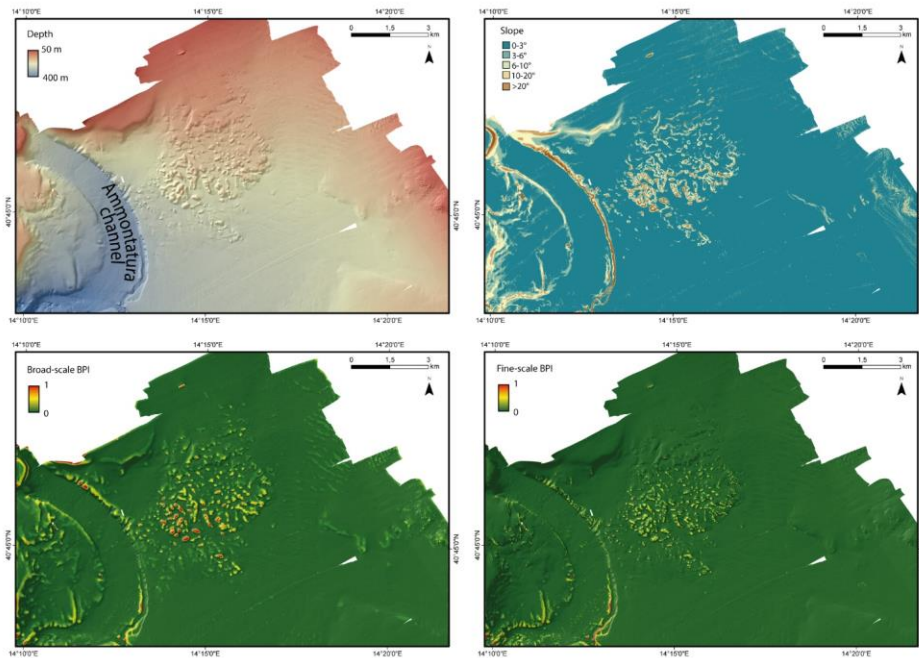
318 Figure 5 (A) Bathymetric data of the Cuma channel; (B) Slope; (C) positive values of broad-scale and (D) fine-scale BPI of a portion of
 319 the area (dashed rectangle in C) calculated from the newly acquired multi-resolution grid.

320 4.1.3 Montagna Bank

321 In the shallower area of the Gulf of Naples, **Montagna Bank** is a morphological high extending over 25 km² (Passaro et al.
 322 2014, 2016, 2018; Ventura et al. 2016), where volcanoclastic materials (dominantly low-density pumice) underwent small-
 323 scale deformation leading to the growth of meter-scale sediment-diapirs and possible fluid-escape features; in particular, this

324 hummocky area includes 280 mounds, 650 cones with meter-scale high, and 30 pockmarks (Sacchi et al., 2019), between
325 100 and 150 m water depth. The slope calculated for the Montagna Bank shows the inclinations of both the whole
326 morphological high and of the individual bedforms surrounding it (i.e., the flanks of the Ammontatura channel and sedimentary
327 bedforms located W of the Montagna Bank). Furthermore, the calculated BPIs reveal large and small mounds constituting the
328 hummocky-like morphology of the large-scale relief.

329



330

331 Figure 6. (A) Bathymetric data of the Montagna Bank; (B) Slope; (C) broad-scale and (D) fine-scale BPI calculated from the newly
332 acquired multi-resolution grid, showing the morphology of the Montagna Bank.

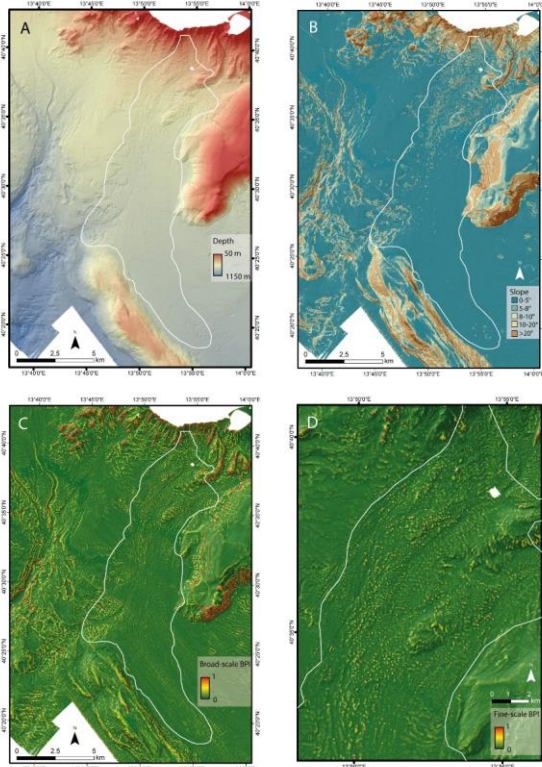
333

334

335 4.1.4 Ischia debris avalanche

336 The Ischia debris-avalanche is located south of Ischia Island and is a 50-km-long tongue characterised by a hummocky
337 topography extending for about 200 km² with fields of giant blocks spanning in size from a few metres to > 200 m across and
338 with larger blocks being up to 30–50 m high (Chiocci and de Alteriis, 2006; de Alteriis et al., 2010). The hummocky deposit

339 follows the local pre-collapse topography, and, on its eastern side, it overflows into the Magnaghi Canyon. The slope (Fig.
340 6B), the broad-scale (Fig. 6C), and fine-scale (Fig. 6D) BPI obtained using different inner and outer rays (Tab. 5), calculated
341 from the newly acquired bathymetric data, allow to better appreciate the morphology of the deposits and clearly identify
342 individual debris blocks, allowing better measurement of their size and volume.
343

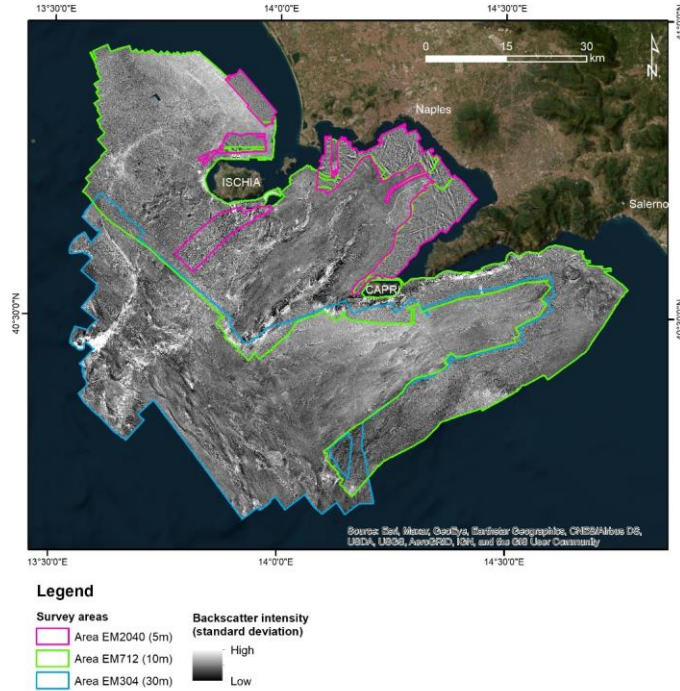


344
345 Figure 7. (A) Bathymetric data of the Ischia Debris Avalanche; (B) Slope; (C) broad-scale and (D) fine-scale BPI calculated from the
346 newly acquired multi-resolution grid, showing the location and morphology of debris blocks. The white square delimitates the area that
347 contains the debris avalanche.
348

349 **4.2 The multi-resolution-grid backscatter mosaic**

350 The backscatter intensity data acquired during the JammeGaia22 cruise represent the first dataset covering the entire Gulf of
351 Naples, Ischia surroundings, Salerno Valley and Sirene Smt. Three mosaics were exported at different spatial resolutions: 5 m
352 for the dataset acquired using the EM2040 system, 10 m for EM712 and 30 m for EM304 (Figure).

353

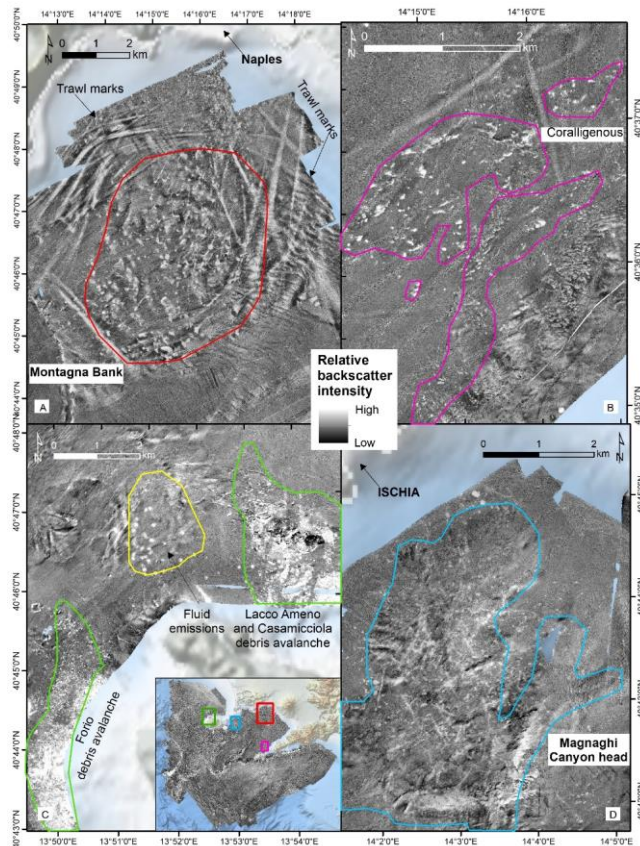


354

355 Figure 8. Backscatter mosaics acquired during the JammeGaia22 cruise with the survey areas covered by the three MBES.

356 Details are shown for four areas: Montagna Bank, Sorrento peninsula, north and west Ischia Island, and Magnaghi canyon
357 head (Figure 8). The backscatter highlighted the hummocky-like morphology of the Montagna Bank and the trawl marks on
358 the seabed around it. The backscatter dataset of the Sorrento peninsula revealed the occurrence of patterns likely associated
359 with coralligenous bioconstructions (the lighter areas) and seagrass meadows along the coast, as previously highlighted in
360 other studies (CARG - Geological CARTography project; EMODnet Seagrass cover (Essential Ocean Variable) in European
361 waters (2023); Russo et al. 2008; Buonocore et al., 2020). Also, the hummocky morphology of the debris avalanches occurring

362 north and west of Ischia Island is enhanced by the seabed reflectivity, together with features of fluid escapes (white spots in
 363 Figure 8C) around Ischia Island and in the head of the Magnaghi canyon, due to the hydrothermal activity characterizing the
 364 area.
 365



366
 367 Figure 9. Details of the seabed backscatter in different locations: A) Montagna Bank hummocky morphology and trawl marks (EM2040 –
 368 5m); B) Coralligenous bioconstructions west of the Sorrento peninsula (EM712 – 10m); C) debris avalanches north and west of Ischia
 369 Island and fluid escape features (EM712 – 10m); D) head of the Magnaghi Canyon characterized by fluid escape features, trawl marks and
 370 areas potentially hosting cold-water corals (EM712 – 10m).
 371

372 **4.3 MBES data quality**

373 The uncertainty of the bathymetric data was calculated in Qimera v.2.5.4 according to the IHO Standards for Hydrographic
 374 Surveys 2-44 6th Edition, 2022. Total Horizontal Uncertainty (THU) and Total Vertical Uncertainty (TVU) were calculated
 375 considering the standard deviation offsets of the MRU, MBES, sound velocity probe, and positioning system. Parameters used
 376 for the calculation of THU and TVU were taken from the datasheet of the MBES systems and installation report (Table 6).
 377 The uncertainty values of EM2040 vary depending on the sampling frequency and depth changes during the survey. Hence,
 378 the values presented below are the range of uncertainty calculated for 200 kHz and 300 kHz and different pulse lengths that
 379 were used during acquisition.

380

381 Table 6. Parameters used to calculate Total Horizontal Uncertainty and Total Vertical Uncertainty

	EM2040	EM712	EM304
Echosounder			
Pulse Length	2, 3, 6, and 12 ms	2 ms	7.5 ms
Sampling Frequency	200kHz, 300 kHz,	70 kHz	25 kHz
Sound Velocity			
SD Surface sound speed	0.02 m/s	0.02 m/s	0.02 m/s
Beam Width			
Beam Width Along (Tx)	0.4°	0.5°	1.0°
Beam Width Across (Rx)	0.7°	1.0°	1.0°
Offsets (Argo)			
SD Roll Offset	0.04°	0.04°	0.04°
SD Pitch Offset	0.02°	0.02°	0.02°
SD Heading Offset	0.02°	0.02°	0.02°
POS			
SD Horizontal	0.1 m	0.1 m	0.1 m
SD Vertical	0.1 m	0.1 m	0.1 m

382

383 Although the scope of our survey was not related to navigation safety, we evaluated whether the horizontal uncertainty (THU)
 384 and vertical uncertainty (TVU) values met the IHO Standards for Hydrographic Surveys 2-44 6th Edition, 2022. Since we
 385 operated deep areas and the underkeel clearance was not an issue, THU and TVU were compared with the Maximum Allowable
 386 THU and TVU calculated at the minimum depth sampled for each MBES according to IHO Standards for Order 2 and 1b.

387 The results show the lowest horizontal uncertainty for data collected using EM2040 (THU = 1.66 to 4.94 m), while those
 388 collected with EM304 present the highest uncertainty (THU = 20.03 m) (Table 7). The lowest vertical uncertainty was obtained
 389 for EM712 (TVU= 1.29 m), whilst the highest for EM2040 (TVU = 4.77 m).

390 The estimated THUs and TVUs of EM712 and EM304 were below their Maximum Allowable values for both Orders 2 and 1.

391 The TVU calculated for the EM2040 is above its Maximum Allowable value for Orders 2 and 1. However, the quality of the

392 data acquired was high enough to produce high-resolution bathymetry and for the scopes of our survey. Uncertainties of the
 393 collected data for all the systems fell within the limits of the IHO Standards for a specific water depth or Order number.

398 Table 7. Mean horizontal and vertical uncertainties of bathymetric data collected using different multibeam systems, and the accepted IHO
 399 error limits, which shows that the data collected are within the IHO standards.

	<u>THU (m)</u>	<u>TVU (m)</u>	<u>Order 2</u>	<u>Order 1</u>	<u>Order 2</u>	<u>Order 1</u>
			<u>Maximum</u>	<u>Maximum</u>	<u>Maximum</u>	<u>Maximum</u>
			<u>Allowable THU</u>	<u>Allowable THU</u>	<u>Allowable TVU</u>	<u>Allowable TVU</u>
			<u>(m)</u>	<u>(m)</u>	<u>(m)</u>	<u>(m)</u>
<u>EM2040</u>	<u>1.66 - 4.94</u>	<u>0.88 - 4.77</u>	<u>25 at 50m</u>	<u>7.5 at 50m</u>	<u>1.52 at 50m</u>	<u>0.82 at 50m</u>
<u>EM712</u>	<u>8.98</u>	<u>1.29</u>	<u>35 at 150m</u>	<u>12.5 at 150m</u>	<u>3.29 at 150m</u>	<u>2.01 at 150m</u>
<u>EM304</u>	<u>20.03</u>	<u>3.67</u>	<u>120 at 1000m</u>	<u>55 at 1000m</u>	<u>23.02 at 1000m</u>	<u>13.01 at 1000m</u>

<u>THU (m)</u>	<u>TVU (m)</u>	<u>IHO S44 6th Order Error Limit</u>	<u>IHO S44 6th Order No.</u>
<u>EM2040</u>	<u>1.66 - 4.94</u>	<u>0.88 - 4.77</u>	<u>2.57</u>
<u>EM712</u>	<u>8.98</u>	<u>1.29</u>	<u>5.28</u>
<u>EM304</u>	<u>20.03</u>	<u>3.67</u>	<u>22.80</u>

403 The uncertainty values calculated for JammeGaia22 survey data testify that the seafloor map of the Gulf of Naples obtained
 404 with the innovative-new technologies installed on board the R/V Gaia Blu represents a product of high quality. This new
 405 dataset will serve as a crucial baseline for future in-depth analysis of the geomorphology of the area, favoring the identification
 406 of seabed features at unprecedented resolution.

407 A significant improvement in the resolution of the data appears evident when comparing the morphology of the Ischia debris
 408 avalanche from DTM at 20 m horizontal resolution generated from the ancient and modern datasets. The newly acquired
 409 dataset shows better coverage and less noise than the 2001 dataset (Figure 9). The blocks of the landslide deposit can be also
 410 clearly identified in the new dataset whilst the identification is not obvious for some areas in the 2001 dataset.

411 To test if this increase in the resolution has an impact on geomorphological indices derived from the bathymetry, we calculated
 412 the fine-scale BPI from the 20 m-resolution DTMs (2001 and the JammeGaia22 surveys) using the same parameters for both
 413 the datasets, reported in Table 5. The results show a much higher noise level for the 2001 DTM with respect to the
 414 JammeGaia22 dataset (Figure 10). The noise was higher especially at the overlap among the swaths on the western part of the

415 dataset, and the central beams of the swath in the central part of the data, where most of the landslide blocks occur. Such blocks
416 are better detected and isolated through BPIs in 2022 DTM, rather than in 2001 DTM.

417

418 **4.4 Comparison to previous data**

419 The area for this study was selected not only for its intriguing dynamic, tectonic and volcanic activity, benthic boundary
420 processes and seafloor biodiversity, and widespread human impacts of various origins. An additional reason was offered by
421 the opportunity to compare the newly acquired data with a previous high-standard multibeam study of the area. In fact, this
422 area has been already mapped since the late '90s with state of the art (for that time) instrumentation and presented in extremely
423 accurate ~~and imaginative~~ 3D views (D'Argenio et al., 2004; de Alteriis et al., 2010; Passaro et al., 2014; Sacchi et al., 2014;
424 Budillon et al., 2016; Paoletti et al., 2016; Passaro et al., 2016a, 2016b; Di Martino et al., 2021; Aiello and Sacchi, 2022). The
425 limitation of that original database came from the need to acquire the data in a succession of surveys spanning several years
426 and using instruments with rather variable resolutions. Nevertheless, also thanks to the extreme accuracy of the data processing
427 performed at that time, this 20-year-old database provided an excellent basis for comparison with the newly acquired, more
428 homogenous, database. Of course, the comparison cannot be pushed to the highest resolution offered by the modern
429 instruments on Gaia Blu but, even on lower resolution, the comparison among 20 m grids from the two data sets can be
430 extremely valuable.

431

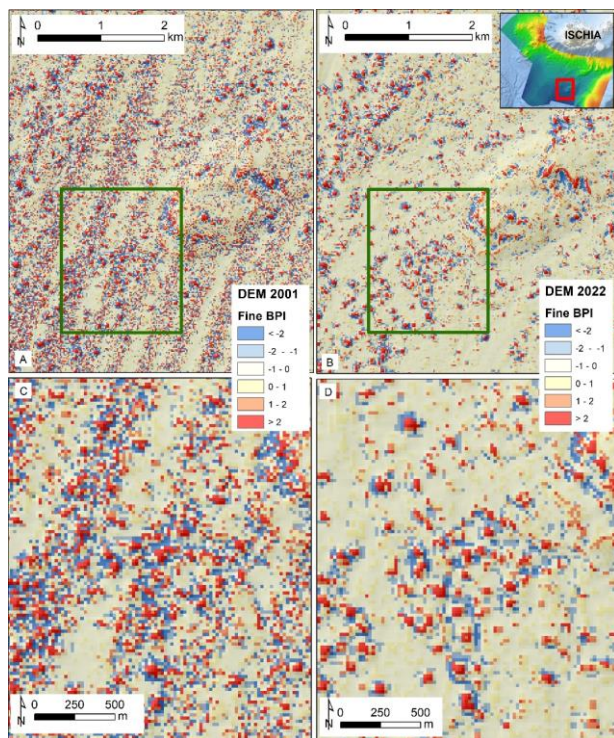


Figure 10. Fine-scale BPI calculated on the 2001 DTM (A) and JammeGaia22 DTM (B) for the area of the Ischia debris avalanche; noticeably, the 2001 dataset is very noisy. Detail of the blocks accumulation for 2001 DTM (C) and JammeGaia22 DTM (D): despite both datasets have same spatial resolution (20 m), the newly acquired dataset allows to better discriminate and map blocks.

5. Data availability

All datasets, products and web services are managed through the ISMAR Marine Spatial Data Infrastructure – MSDI (Foglini & Grande 2023) and follow the ISMAR-CNR Data policy (<https://doi.org/10.26383/CNR-ISMAR.2023.6>). Bathymetric datasets gathered by the MBES in the format GSF (generic sensor format), and bathymetric and backscatter surfaces (GeoTIFF) are shared in the Marine Geoscience Data System (MGDS) (Table 8).

443 Data are also available as Web Map Services (WMS), that are interoperable with other infrastructures and permit the integration
 444 of the spatial data in other geoportals or directly in a desktop environment (e.g., QGIS, ArcMap). Data are free ly accessible
 445 thought two main interfaces: the metadata catalogue and the WebGIS.

446 The CNR-ISMAR GeoNetwork metadata catalogue ([http://seamap-](http://seamap-catalog.data.ismar.cnr.it:8080/geonetwork)
 447 [catalog.data.ismar.cnr.it:8080/geonetworkhttps://www.ismar.cnr.it/en/infrastructures/information_resources/geo_portals/#2](https://www.ismar.cnr.it/en/infrastructures/information_resources/geo_portals/#2))
 448 allows users to find the JammeGaia22 products (refer to Table 8 for direct links to products),containing information about
 449 access and use policy, link to download the data, how to cite the data, DOI, and links to external repositories (such as EMODnet
 450 and MGDS). The WebGIS ([http://seamap-](http://seamap-explorer.data.ismar.cnr.it:8080/mokaApp/applicazioni/ismarBoApp)
 451 [explorer.data.ismar.cnr.it:8080/mokaApp/applicazioni/ismarBoApphttps://www.ismar.cnr.it/en/infrastructures/information-](https://www.ismar.cnr.it/en/infrastructures/information_resources/geo_portals/#1)
 452 [resources/geo_portals/#1](https://www.ismar.cnr.it/en/infrastructures/information_resources/geo_portals/#1)) publishes survey areas, multibeam navigation lines, bathymetric surfaces and backscatter mosaics.
 453 Users can navigate the map to the JammeGaia22 survey area, explore the layer list and open the geophysical data and products.
 454 By clicking on spatial objects on the map, users can access the related information, such as the download link.

455 Table 8. Products of the JammeGaia22 oceanographic cruise with relative link.

Product	Typology	Depth range	Spatial resolution	Format	Link CNR-ISMAR Catalog	DOIs
Survey JAMME GAIA 2022	Cruise report	-	-	PDF	http://libeccio.bo.ismar.cnr.it:8080/geonetwork/srv/eng/catalog.search#/metadata/6cd1080c-f41f-4c9d-907b-297d25f554e5	Foglini, et al., 2024a, https://doi.org/10.26383/CNR-ISMAR.2024.4
JG22_SwathLines_EM2040	MBES processed lines	-	-	GSF	http://libeccio.bo.ismar.cnr.it:8080/geonetwork/srv/eng/catalog.search#/metadata/6213658d-ca9a-4e40-af07-e4f7b329203a	Foglini, 2024a http://dx.doi.org/10.60521/331589
JG22_SwathLines_EM712	MBES processed lines	-	-	GSF	http://libeccio.bo.ismar.cnr.it:8080/geonetwork/srv/eng/catalog.search#/metadata/6213658d-ca9a-4e40-af07-e4f7b329203a	Foglini 2024b http://dx.doi.org/10.60521/331587

JG22_SwathLines_EM304	MBES processed lines	-	-	GSF	http://libeccio.bo.ismar.cnr.it:8080/geonetwark/srv/eng/catalog.search#metadata/6213658d-ca9a-4e40-af07-e4f7b329203a	Foglini 2024c, http://dx.doi.org/10.60521/331584
JG22_50_120_2m	Bathymetric surface	50-120 m	2 m	ASCII GeoTIFF ESRI_grid	http://libeccio.bo.ismar.cnr.it:8080/geonetwark/srv/eng/catalog.search#metadata/927334e6-021a-4eed-a0a6-f209df3b17ad	Foglini et al. 2024b, http://dx.doi.org/10.60521/331667
JG22_100_200_5m	Bathymetric surface	100 -200 m	5 m	ASCII GeoTIF ESRI_grid	http://libeccio.bo.ismar.cnr.it:8080/geonetwark/srv/eng/catalog.search#metadata/5e384b50-ea4d-4e68-b023-d5b64ebd5ed8	
JG22_180_500_10m	Bathymetric surface	180-500 m	10 m	ASCII GeoTIFF ESRI_grid	http://libeccio.bo.ismar.cnr.it:8080/geonetwark/srv/eng/catalog.search#metadata/e956cee4-ba1c-41b7-932b-4031932c9a9d	
JG22_480_700_15m	Bathymetric surface	480-700 m	15 m	ASCII GeoTIFF ESRI_grid	http://libeccio.bo.ismar.cnr.it:8080/geonetwark/srv/eng/catalog.search#metadata/5124f1d9-982c-4996-8333-298eb62e5c73	
JG22_680_1000_20m	Bathymetric surface	680-1000 m	20 m	ASCII GeoTIFF ESRI_grid	http://libeccio.bo.ismar.cnr.it:8080/geonetwark/srv/eng/catalog.search#metadata/214811a5-1700-413f-9b3f-95d2ddd29996	

JG22_980_1300_30m	Bathymetric surface	980-1300 m	30 m	ASCII GeoTIFF ESRI_grid	http://libeccio.bo.ismar.cnr.it:8080/geonetwark/srv/eng/catalog/search#metadata/a43cf1d4-abc6-43e4-9f66-fac08827c5dd	
JG22_1280_2120_40m	Bathymetric surface	1280-2120 m	40 m	ASCII GeoTIFF ESRI_grid	http://libeccio.bo.ismar.cnr.it:8080/geonetwark/srv/eng/catalog/search#metadata/96388cc5-2c58-4ba3-9816-7231c69d96e8	
JG22_2040_5m	Backscatter mosaic from EM2040	-	5 m	ASCII GeoTIFF ESRI_grid	http://libeccio.bo.ismar.cnr.it:8080/geonetwark/srv/eng/catalog/search#metadata/6ec52054-ac6c-46e6-966b-8a88d1cf4351	
JG22_712_10m	Backscatter mosaic from EM712	-	10 m	ASCII GeoTIFF ESRI_grid	http://libeccio.bo.ismar.cnr.it:8080/geonetwark/srv/eng/catalog/search#metadata/d4c1635f-69f2-4ebc-9174-d2a9d60a1e58	Fogliini et al. 2024c, http://dx.doi.org/10.60521/331668
JG22_304_30m	Backscatter mosaic from EM304	-	30 m	ASCII GeoTIFF ESRI_grid	http://libeccio.bo.ismar.cnr.it:8080/geonetwark/srv/eng/catalog/search#metadata/94f61db5-c186-48a6-b82b-7d9685c2a541	

456

457 6. Conclusions

458 The JammeGaia22 cruise led to the creation of ~~a multi-resolution~~-DTM and backscatter mosaics at different resolutions for the
459 Gulf of Naples, by using three different state-of-the-art MBESs. The dataset has been obtained through a reproducible
460 processing workflow and corresponds to a major upgrade of a pre-existing bathymetry of the area. The vertical and positioning
461 uncertainties of the bathymetric data fall within the IHO standards and satisfy Order 1b for EM2040 and Order 2 for EM712
462 and EM304.

463 The newly acquired multi beam maps reveal submerged morphologies at a scale and resolution never achieved before for the
464 study area, allowing for a wide range of local and regional studies, spanning from geological and geomorphological research
465 to marine habitat mapping and sea-floor monitoring. Furthermore, these high-resolution bathymetry and backscatter datasets
466 can be useful for many and diverse applications, such as Maritime-maritime spatial Planning-planning and for designing
467 innovative conservation strategies.

468 The new data base is released to the community as a benchmark reference against which future sea-floor changes can be
469 quantified and ascribed to either the activity of subaqueous volcanic apparatuses, in particular in the vicinity of the Flegraean
470 Field, the flux of density flows along major conduits like Cuma Channel, and Magnaghi and Dohrn Canyons, slope instability
471 leading to mass-transport deposits or sand splays at the mouth of slope gullies. Large scale bedforms are particularly developed
472 in regions flow rearrangement like in a bend of Cuma Channel, west of Ischia Island, or in the area of possible cyclic steps, on
473 the slope south of Ischia. Backscatter data help recognizing areas of potential occurrence of white-cold-water coral colonies
474 and coralligenous bioconstructions, a key element of the Mediterranean biodiversity richness. Finally, both bathymetric and
475 backscatter data help define the areas most impacted by fish trawling, smoothing and remoulding the seafloor, fluid escape
476 features and landslidesillegal dumping and diffused littering.

ha formattato: Non Evidenziato

ha formattato: Non Evidenziato

ha formattato: Non Evidenziato

ha formattato: Non Evidenziato

ha formattato: Non Evidenziato

ha formattato: Non Evidenziato

477 7. Author contribution

478 FF: Supervisor, data collection and processing, conceptualisation, and writing; MR: Supervisor, data collection,
479 conceptualisation; RT: Supervisor, data collection and processing; GC, DG: data collection, data processing, first draft writing;
480 VG, MP: data management, data processing, first draft writing; LP, CP, FB, FM, MC, MS, ML, PM data collection and review;
481 GD, SI, ANT, AP, AM, AR data collection and processing; FT: Supervisor and review.

482 8. Competing interests

483 The contact author has declared that none of the authors has any competing interests.

484 9. Acknowledgements

485 We thank captain, crew, and scientific staff of R/V Gaia Blu for their skilful and efficient cooperation during operations at sea.
486 This is ISMAR-Bologna scientific contribution no. 2088.

487 **References**

- 488 Aiello, G., Iorio, M., Molisso, F., and Sacchi, M.: Integrated Morpho-Bathymetric, Seismic-Stratigraphic, and
489 Sedimentological Data on the Dohrn Canyon (Naples Bay, Southern Tyrrhenian Sea): Relationships with
490 Volcanism and Tectonics, *Geosciences*, 10, 319, <https://doi.org/10.3390/geosciences10080319>, 2020.
- 491 Aiello, G., Sacchi, M.: New morpho-bathymetric data on marine hazard in the offshore of Gulf of Naples (Southern
492 Italy). *Natural Hazards* 111(3), 2881-2908, 2022.
- 493 Albert, P. G., Giaccio, B., Isaia, R., Costa, A., Niespolo, E. M., Nomade, S., Pereira, A., Renne, P. R., Hinchliffe,
494 A., Mark, D. F., Brown, R. J., and Smith, V. C.: Evidence for a large-magnitude eruption from Campi Flegrei
495 caldera (Italy) at 29 ka, *Geology*, 47, 595–599, <https://doi.org/10.1130/G45805.1>, 2019.
- 496 Amato, V., Aucelli, P. P. C., Cinque, A., D'Argenio, B., Donato, V. D., Pappone, G., Petrosino, P., Roskopf, C.
497 M., and Ermolli, E. R.: Holocene palaeo-geographical evolution of the Sele river coastal plain (Southern Italy):
498 new morpho-sedimentary data from the Paestum area, *Alpine and Mediterranean Quaternary*, 24, 5–7, 2011.
- 499 Angiolillo, M., Bo, M., Toma, M., Giusti, M., Salvati, E., Giova, A., Lagudi, A., Rossi, L., Collina, M., Bruno, F.,
500 Canese, S., and Tunesi, L.: A baseline for the monitoring of Mediterranean upper bathyal biogenic reefs within the
501 marine strategy framework directive objectives, *Deep Sea Research Part I: Oceanographic Research Papers*, 194,
502 103963, <https://doi.org/10.1016/j.dsr.2023.103963>, 2023.
- 503 Appolloni, L., Sandulli, R., Vetrano, G., and Russo, G. F.: A new approach to assess marine opportunity costs and
504 monetary values-in-use for spatial planning and conservation; the case study of Gulf of Naples, Mediterranean Sea,
505 *Italy, Ocean & Coastal Management*, 152, 135–144, <https://doi.org/10.1016/j.ocecoaman.2017.11.023>, 2018.
- 506 Appolloni, L., Zeppilli, D., Donnarumma, L., Baldrighi, E., Chianese, E., Russo, G., and Sandulli, R.: Seawater
507 Acidification Affects Beta-Diversity of Benthic Communities at a Shallow Hydrothermal Vent in a Mediterranean
508 Marine Protected Area (Underwater Archaeological Park of Baia, Naples, Italy), *Diversity*, 12, 464,
509 <https://doi.org/10.3390/d12120464>, 2020.
- 510 Basterretxea, G., Font-Muñoz, J. S., Salgado-Hernanz, P. M., Arrieta, J., and Hernández-Carrasco, I.: Patterns of
511 chlorophyll interannual variability in Mediterranean biogeographical regions, *Remote Sensing of Environment*,
512 215, 7–17, <https://doi.org/10.1016/j.rse.2018.05.027>, 2018.
- 513 Bavestrello, G., Bo, M., Canese, S., Sandulli, R., and Cattaneo-Vietti, R.: The red coral populations of the gulfs of
514 Naples and Salerno: human impact and deep mass mortalities, *Italian Journal of Zoology*, 81, 552–563,
515 <https://doi.org/10.1080/11250003.2014.950349>, 2014.
- 516 Beaudoin, J., Renoud, W., Mohammadloo, T. H., & Snellen, M. Automated correction of refraction residuals. In
517 HYDRO18 conference, 2018.
- 518 Bellucci, F., Milia, A., Rolandi, G., and Torrente, M. M.: Chapter 8 Structural control on the Upper Pleistocene
519 ignimbrite eruptions in the Neapolitan area (Italy): volcano tectonic faults versus caldera faults, in: *Developments*
520 *in Volcanology*, vol. 9, edited by: De Vivo, B., Elsevier, 163–180, [https://doi.org/10.1016/S1871-644X\(06\)80022-](https://doi.org/10.1016/S1871-644X(06)80022-7)
521 [7](https://doi.org/10.1016/S1871-644X(06)80022-7), 2006.

- 522 Bianchi, C. N. and Morri, C.: Marine Biodiversity of the Mediterranean Sea: Situation, Problems and Prospects for
523 Future Research, *Marine Pollution Bulletin*, 40, 367–376, [https://doi.org/10.1016/S0025-326X\(00\)00027-8](https://doi.org/10.1016/S0025-326X(00)00027-8), 2000.
- 524 Budillon, F., Violante, C., De Lauro M. I fondali delle Isole Flegree, morfologia e geologia. in: *Ambiente marino*
525 *costiero e territorio delle isole flegree (Ischia Procida e Vivara – Golfo di Napoli)*. Risultati di uno studio
526 multidisciplinare, edited by: Gambi, M. C., De Lauro, M., Jannuzzi, F., *Mem. Acc. Sci. Fis. E Matem.*, Napoli 5,
527 45-66, 2003.
- 528 Budillon, F., Cesarano, M., Conforti, A., Pappone, G., Di Martino, G., Pelosi, N.: Recurrent superficial sediment
529 failure and deep gravitational deformation in a Pleistocene slope marine succession: The *Poseidonia* slide (Salerno
530 Bay, Tyrrhenian Sea), *Submarine Mass Movements and Their Consequences*, 6th International Symposium, 273-
531 283, 2016.
- 532 Budillon F., Firetto Carlino M., Innangi S., Passaro S., Tonielli R., Trincardi F., Sprovieri M. ~~(2022)~~: The
533 Anthropogenic Footprint of Physical Harm on the Seabed of Augusta Bay (Western Ionian Sea). *Journal of Marine*
534 *Science and Engineering* 10 (11), 1737. Buonocore, E., Appolloni, L., Russo, G. F., and Franzese, P. P.: Assessing
535 natural capital value in marine ecosystems through an environmental accounting model: A case study in Southern
536 Italy, *Ecological Modelling*, 419, 108958, <https://doi.org/10.1016/j.ecolmodel.2020.108958>, 2020.
- 537 [Burrough, P. A., and McDonell, R. A: Principles of Geographical Information Systems. Oxford University Press,](#)
538 [New York, 120 pp., 1998.](#)
- 539 Canals, M., Pham, C. K., Bergmann, M., Gutow, L., Hanke, G., Seville, E. van, Angiolillo, M., Buhl-Mortensen,
540 L., Cau, A., Ioakeimidis, C., Kammann, U., Lundsten, L., Papatheodorou, G., Purser, A., Sanchez-Vidal, A.,
541 Schulz, M., Vinci, M., Chiba, S., Galgani, F., Langenkämper, D., Möller, T., Nattkemper, T. W., Ruiz, M.,
542 Suikkanen, S., Woodall, L., Fakiris, E., Jack, M. E. M., and Giorgetti, A.: The quest for seafloor macrolitter: a
543 critical review of background knowledge, current methods and future prospects, *Environ. Res. Lett.*, 16, 023001,
544 <https://doi.org/10.1088/1748-9326/abc6d4>, 2021.
- 545 CARG (Geological CARTography) project: [https://www.isprambiente.gov.it/en/projects/soil-and-territory/carg-](https://www.isprambiente.gov.it/en/projects/soil-and-territory/carg-project-geologic-and-geothematic-cartography)
546 [project-geologic-and-geothematic-cartography](https://www.isprambiente.gov.it/en/projects/soil-and-territory/carg-project-geologic-and-geothematic-cartography) (last access: 28 February 2024)
- 547 Chiocci, F. L. and De Alteriis, G.: The Ischia debris avalanche: first clear submarine evidence in the Mediterranean
548 of a volcanic island prehistorical collapse, *Terra Nova*, 18, 202–209, [https://doi.org/10.1111/j.1365-](https://doi.org/10.1111/j.1365-3121.2006.00680.x)
549 [3121.2006.00680.x](https://doi.org/10.1111/j.1365-3121.2006.00680.x), 2006.
- 550 Coll, M., Piroddi, C., Albouy, C., Ben Rais Lasram, F., Cheung, W. W. L., Christensen, V., Karpouzi, V. S.,
551 Guilhaumon, F., Mouillot, D., Paleczny, M., Palomares, M. L., Steenbeek, J., Trujillo, P., Watson, R., and Pauly,
552 D.: The Mediterranean Sea under siege: spatial overlap between marine biodiversity, cumulative threats and marine
553 reserves, *Global Ecology and Biogeography*, 21, 465–480, <https://doi.org/10.1111/j.1466-8238.2011.00697.x>,
554 2012.
- 555 D’Argenio, B., Angelino, A., Aiello, G., de Alteriis, G., Milia, A., Sacchi, M., Tonielli, R., Budillon, F., Chiocci,
556 F. L., Conforti, A., Lauro, M., Di Martino, G., D’Isanto, C., Esposito, E., Ferraro, L., Innangi, S., Insinga, D. D.,
557 Iorio, Marsella, E., Molisso, F., Morra, V. B., Passaro, S., Pelosi, N., Pordo, S., Raspini, A., Ruggieri, S.,
558 Sarnacchiaro, G., Terranova, C., Vilardo, G., and Violante, C.: Digital elevation model of the Naples Bay and

ha formattato: Inglese (Stati Uniti)

559 adjacent areas (Eastern Tyrrhenian Sea), in: Mapping Geology in Italy, Atlante di Cartografia Geologica, vol.
560 Convegno Internazionale Firenze, edited by: Pasquarè, E. and Venturini, G., Firenze, Italy, 21–28, 2004.

561 de Alteriis, G., Insinga, D. D., Morabito, S., Morra, V., Chiocci, F. L., Terrasi, F., Lubritto, C., Di Benedetto, C.,
562 and Pazzanese, M.: Age of submarine debris avalanches and tephrostratigraphy offshore Ischia Island, Tyrrhenian
563 Sea, Italy, *Marine Geology*, 278, 1–18, <https://doi.org/10.1016/j.margeo.2010.08.004>, 2010.

564 Deino, A. L., Orsi, G., de Vita, S., and Piochi, M.: The age of the Neapolitan Yellow Tuff caldera-forming eruption
565 (Campi Flegrei caldera – Italy) assessed by 40Ar/39Ar dating method, *Journal of Volcanology and Geothermal*
566 *Research*, 133, 157–170, [https://doi.org/10.1016/S0377-0273\(03\)00396-2](https://doi.org/10.1016/S0377-0273(03)00396-2), 2004.

567 Díaz, S., Settele, J., Brondízio, E. S., Ngo, H. T., Agard, J., Arneth, A., Balvanera, P., Brauman, K. A., Butchart,
568 S. H. M., Chan, K. M. A., Garibaldi, L. A., Ichii, K., Liu, J., Subramanian, S. M., Midgley, G. F., Miloslavich, P.,
569 Molnár, Z., Obura, D., Pfaff, A., Polasky, S., Purvis, A., Razzaque, J., Reyers, B., Chowdhury, R. R., Shin, Y.-J.,
570 Visseren-Hamakers, I., Willis, K. J., and Zayas, C. N.: Pervasive human-driven decline of life on Earth points to
571 the need for transformative change, *Science*, 366, eaax3100, <https://doi.org/10.1126/science.aax3100>, 2019.

572 Di Martino, G., Innangi, S., Sacchi, M., Tonielli, R.: Seafloor morphology changes in the inner-shelf area of the
573 Pozzuoli Bay, Eastern Tyrrhenian Sea, *Marine Geophysical Research*, 42(2),13, 2021.

574 Dolan, M. F. J.: Calculation of slope angle from bathymetry data using GIS - effects of computation algorithm,
575 data resolution and analysis scale, [Geological Survey of Norway Report No. 2012.041, 40 pp., 2012](#)
576 ~~2012~~.

577 Donnarumma, L., Appolloni, L., Chianese, E., Bruno, R., Baldrighi, E., Guglielmo, R., Russo, G. F., Zeppilli, D.,
578 and Sandulli, R.: Environmental and Benthic Community Patterns of the Shallow Hydrothermal Area of Secca
579 Delle Fumose (Baia, Naples, Italy), *Front. Mar. Sci.*, 6, 685, <https://doi.org/10.3389/fmars.2019.00685>, 2019.

580 EMODnet Seagrass cover (Essential Ocean Variable) in European waters (2023):
581 [https://emodnet.ec.europa.eu/geonetwork/emodnet/eng/catalog.search#/metadata/39746d9c-4220-425c-bc26-](https://emodnet.ec.europa.eu/geonetwork/emodnet/eng/catalog.search#/metadata/39746d9c-4220-425c-bc26-7cb3056c36a5)
582 [7cb3056c36a5](https://emodnet.ec.europa.eu/geonetwork/emodnet/eng/catalog.search#/metadata/39746d9c-4220-425c-bc26-7cb3056c36a5) (last access: 28 February 2024).

583 Foglini, F. Processed EM2040 Acoustic Backscatter and Swath Bathymetry data from R/V Gaia Blu cruise Jamme
584 Gaia22 (2022). MGDS. 2024a, doi:10.60521/331589

585 Foglini, F. Processed EM712 Acoustic Backscatter and Swath Bathymetry data from R/V Gaia Blu cruise Jamme
586 Gaia22 (2022). MGDS. 2024b, doi:[10.60521/331587](https://doi.org/10.60521/331587)

587 Foglini, F. Processed EM304 Acoustic Backscatter and Swath Bathymetry data from R/V Gaia Blu cruise Jamme
588 Gaia22 (2022). MGDS. 2024c, doi:[10.60521/331584](https://doi.org/10.60521/331584)

589 Foglini, F. and Grande, V.: A Marine Spatial Data Infrastructure to manage multidisciplinary, inhomogeneous and
590 fragmented geodata in a FAIR perspective ... the Adriatic Sea experience, *Oceanologia*, 65, 260–277,
591 <https://doi.org/10.1016/j.oceano.2022.11.002>, 2023.

592 Foglini, F., Tonielli, R., and Rovere M. Cruise report Survey JAMME GAIA 2022. CNR-ISMAR, 2024a,
593 <https://doi.org/10.26383/CNR-ISMAR.2024.4>

594 Foglini, F.; Tonielli, R. and M. Rovere. Multi-Resolution bathymetry grids of the Naples and Pozzuoli Gulf and
595 the Amalfi Coastal Area collected during cruise Jamme_Gaia22, 2022. MGDS. 2024b, doi:[10.60521/331667](https://doi.org/10.60521/331667)

596 Foglini, F.; Tonielli, R. and M. Rovere. Multi-Resolution backscatter grids of the Naples and Pozzuoli Gulf and
597 the Amalfi Coastal Area collected during cruise Jamme_Gaia22, 2022. MGDS, 2024c,
598 doi:10.60521/331668Giaccio, B., Isaia, R., Fedele, F. G., Di Canzio, E., Hoffecker, J., Ronchitelli, A., Sinitsyn, A.
599 A., Anikovich, M., Lisitsyn, S. N., and Popov, V. V.: The Campanian Ignimbrite and Codola tephra layers: Two
600 temporal/stratigraphic markers for the Early Upper Palaeolithic in southern Italy and eastern Europe, *Journal of*
601 *Volcanology and Geothermal Research*, 177, 208–226, <https://doi.org/10.1016/j.jvolgeores.2007.10.007>, 2008.

602 Giaccio B., Hajdas I., Isaia R., Deino A., Nomade S. High-precision ¹⁴C and ⁴⁰Ar/³⁹Ar dating of the Campanian
603 Ignimbrite (Y-5) reconciles the time-scales of climatic-cultural processes at 40 ka. *Sci. Rep.* 7, 45940; doi:
604 [10.1038/srep45940](https://doi.org/10.1038/srep45940), 2017.

605 Iampietro, P. and Kvittek, R.: Iampietro, P., and R. Kvittek. 2002. Quantitative seafloor habitat classification using
606 GIS terrain analysis: Effects of data density, resolution, and scale. In *Proceedings of the 22nd Annual ESRI User*
607 *Conference*. San Diego, CA July 8–12, in: *Proceedings of the 22nd Annual ESRI User Conference*, 22nd Annual
608 *ESRI User Conference*, San Diego, CA, 2002.

609 Isaia, R., Vitale, S., Marturano, A., Aiello, G., Barra, D., Ciarcia, S., Iannuzzi, E., and Tramparulo, F. D.: High-
610 resolution geological investigations to reconstruct the long-term ground movements in the last 15 kyr at Campi
611 Flegrei caldera (southern Italy), *Journal of Volcanology and Geothermal Research*, 385, 143–158,
612 <https://doi.org/10.1016/j.jvolgeores.2019.07.012>, 2019.

613 Kastens, K., Mascle, J., Auroux, C., Bonatti, E., Broglia, C., Channell, J., Curzi, P., Emeis, K.-C., Glaçon, G.,
614 Hasegawa, S., Hieke, W., Mascle, G., McCoy, F., McKenzie, J., Mendelson, J., Müller, C., Réhault, J.-P.,
615 Robertson, A., Sartori, R., Sprovieri, R., and Torii, M.: ODP Leg 107 in the Tyrrhenian Sea: Insights into passive
616 margin and back-arc basin evolution, *GSA Bulletin*, 100, 1140–1156, [https://doi.org/10.1130/0016-](https://doi.org/10.1130/0016-7606(1988)100<1140:OLITTS>2.3.CO;2)
617 [7606\(1988\)100<1140:OLITTS>2.3.CO;2](https://doi.org/10.1130/0016-7606(1988)100<1140:OLITTS>2.3.CO;2), 1988.

618 Kostic, S.: Modeling of submarine cyclic steps: controls on their formation, migration, and architecture. *Geosphere*,
619 7(2), 294-304, 2011.

620 Le Bas, T. P. RSOBIA: A new OBIA Toolbar and Toolbox in ArcMap 10.x for Segmentation and Classification,
621 in: *Proceedings of GEOBIA 2016 : Solutions and synergies*, 14-16 September 2016, Enschede, Netherlands, 6th
622 *International Conference on Geographic Object-Based Image Analysis*, GEOBIA 2016: Solutions & Synergies,
623 <https://doi.org/10.3990/2.448>, 2016.

624 Loreto, M. F., Zitellini, N., Ranero, C. R., Palmiotto, C., and Prada, M.: Extensional tectonics during the Tyrrhenian
625 back-arc basin formation and a new morpho-tectonic map, *Basin Research*, 33, 138–158,
626 <https://doi.org/10.1111/bre.12458>, 2021.

627 Lucchi, F. R., Colella, A., Gabbianelli, G., Rossi, S., & Normark, W. R.: The Crati submarine fan, Ionian sea. *Geo-*
628 *marine letters*, 3, 71-77, 1983.

Codice campo modificato

- 629 Lundblad, E. R., Wright, D. J., Miller, J., Larkin, E. M., Rinehart, R., Naar, D. F., Donahue, B. T., Anderson, S.
630 M., and Battista, T.: A Benthic Terrain Classification Scheme for American Samoa, *Marine Geodesy*, 29, 89–111,
631 <https://doi.org/10.1080/01490410600738021>, 2006.
- 632 Lymer, G., Lofi, J., Gaullier, V., Maillard, A., Thinon, I., Sage, F., Chanier, F., and Vendeville, B. C.: The Western
633 Tyrrhenian Sea revisited: New evidence for a rifted basin during the Messinian Salinity Crisis, *Marine Geology*,
634 398, 1–21, <https://doi.org/10.1016/j.margeo.2017.12.009>, 2018.
- 635 Madricardo, F., Fogliani, F., Campiani, E., Grande, V., Catenacci, E., Petrizzo, A., Kruss, A., Toso, C., and
636 Trincardi, F.: Assessing the human footprint on the sea-floor of coastal systems: the case of the Venice Lagoon,
637 Italy, *Sci Rep*, 9, 6615, <https://doi.org/10.1038/s41598-019-43027-7>, 2019.
- 638 Marine Geoscience Data System – MGDS: <https://www.marine-geo.org/> (last access: 28 February 2024).
- 639 Mattei, G., Rizzo, A., Anfuso, G., Aucelli, P. P. C., and Gracia, F. J.: A tool for evaluating the archaeological
640 heritage vulnerability to coastal processes: The case study of Naples Gulf (southern Italy), *Ocean & Coastal*
641 *Management*, 179, 104876, <https://doi.org/10.1016/j.ocecoaman.2019.104876>, 2019.
- 642 Mayer, L., Jakobsson, M., Allen, G., Dorschel, B., Falconer, R., Ferrini, V., Lamarche, G., Snaith, H., and
643 Weatherall, P.: The Nippon Foundation—GEBCO Seabed 2030 Project: The Quest to See the World’s Oceans
644 Completely Mapped by 2030, *Geosciences*, 8, 63, <https://doi.org/10.3390/geosciences8020063>, 2018.
- 645 Milia, A.: Aggrading and prograding infill of a peri-Tyrrhenian Basin (Naples Bay, Italy), *Geo-Marine Letters*, 19,
646 237–244, <https://doi.org/10.1007/s003670050114>, 1999.
- 647 Milia, A.: The Dohrn canyon: a response to the eustatic fall and tectonic uplift of the outer shelf along the eastern
648 Tyrrhenian Sea margin, Italy, *Geo-Marine Letters*, 20, 101–108, <https://doi.org/10.1007/s003670000044>, 2000.
- 649 Milia, A., Torrente, M. M., Russo, M., and Zuppetta, A.: Tectonics and crustal structure of the Campania
650 continental margin: relationships with volcanism, *Mineralogy and Petrology*, 79, 33–47,
651 <https://doi.org/10.1007/s00710-003-0005-5>, 2003.
- 652 Miramontes, E., Déverchère, J., Pellegrini, C., & Chiarella, D.: Mediterranean Sea evolution and present-day
653 physiography. In *Oceanography of the Mediterranean Sea* (pp. 13-39). Elsevier, 2023.
- 654 Mohammadloo, T. H., Snellen, M., Renoud, W., Beaudoin, J., and Simons, D. G.: Correcting Multibeam
655 Echosounder Bathymetric Measurements for Errors Induced by Inaccurate Water Column Sound Speeds, *IEEE*
656 *Access*, 7, 122052–122068, <https://doi.org/10.1109/ACCESS.2019.2936170>, 2019.
- 657 Moussat, E., Rehault, J.-P., Fabbri, A., and Mascle, G.: Evolution géologique de la Mer Tyrrhénienne, [Comptes](https://doi.org/10.1016/j.crs.1985.01.001)
658 [Rendus de l’Académie des Sciences, Paris, 301, série II, 7: 491–496., 1985C. r. Acad. sci., Sér. 2, Mée. phys. chim.](https://doi.org/10.1016/j.crs.1985.01.001)
659 [sci. univers sci. terre, 301, 491–496, 1985.](https://doi.org/10.1016/j.crs.1985.01.001)
- 660 Myers, N., Mittermeier, R. A., Mittermeier, C. G., da Fonseca, G. A. B., and Kent, J.: Biodiversity hotspots for
661 conservation priorities, *Nature*, 403, 853–858, <https://doi.org/10.1038/35002501>, 2000.

- 662 Orsi, G., D'Antonio, M., Vita, S. de, and Gallo, G.: The Neapolitan Yellow Tuff, a large-magnitude trachytic
663 phreatoplinian eruption: eruptive dynamics, magma withdrawal and caldera collapse, *Journal of Volcanology and*
664 *Geothermal Research*, 53, 275–287, [https://doi.org/10.1016/0377-0273\(92\)90086-S](https://doi.org/10.1016/0377-0273(92)90086-S), 1992.
- 665 Passaro, S., Genovese, S., Sacchi, M., Barra, M., Rumolo, P., Tamburrino, S., Mazzola, S., Basilone, G., Placenti,
666 F., Aronica, S., and Bonanno, A.: First hydroacoustic evidence of marine, active fluid vents in the Naples Bay
667 continental shelf (Southern Italy), *Journal of Volcanology and Geothermal Research*, 285, 29–35,
668 <https://doi.org/10.1016/j.jvolgeores.2014.08.001>, 2014.
- 669 Passaro, S., Tamburrino, S., Vallefucio, M., Tassi, F., Vaselli, O., Giannini, L., Chiodini, G., Caliro, S., Sacchi,
670 M., Luca Rizzo, A., et al. Seafloor doming driven by degassing processes unveils sprouting volcanism in coastal
671 areas. *Sci. Rep.*, 6, 22448, 2016.
- 672 Passaro, S., Sacchi, M., Tamburrino, S., and Ventura, G.: Fluid Vents, Flank Instability, and Seafloor Processes
673 along the Submarine Slopes of the Somma-Vesuvius Volcano, Eastern Tyrrhenian Margin, *Geosciences*, 8, 60,
674 <https://doi.org/10.3390/geosciences8020060>, 2018.
- 675 Pellegrini, C., Saliu, F., Bosman, A., Sammartino, I., Raguso, C., Mercorella, A., & Rovere, M.: Hotspots of
676 microplastic accumulation at the land-sea transition and their spatial heterogeneity: The Po River prodelta (Adriatic
677 Sea). *Science of The Total Environment*, 895, 164908, <https://doi.org/10.1016/j.scitotenv.2023.164908>, 2023.
- 678 Puig, P., Canals, M., Company, J. B., Martín, J., Amblas, D., Lastras, G., Palanques, A., and Calafat, A. M.:
679 Ploughing the deep sea floor, *Nature*, 489, 286–289, <https://doi.org/10.1038/nature11410>, 2012.
- 680 R Core Team: *R: A Language and Environment for Statistical Computing*, Vienna, Austria, 2019.
- 681 Romano, P., Santo, A., Voltaggio, M. L'evoluzione geomorfologia della Pianura del fiume Volturno (Campania)
682 durante il tardo Quaternario (Pleistocene medio-superiore/Olocene). *Il Quaternario* 7(1): 41–56, 1984.
- 683 Ruberti, D., Buffardi, C., Sacchi, M., and Vigliotti, M.: The late Pleistocene-Holocene changing morphology of
684 the Volturno delta and coast (northern Campania, Italy): Geological architecture and human influence, *Quaternary*
685 *International*, 625, 14–28, <https://doi.org/10.1016/j.quaint.2022.03.023>, 2022.
- 686 Russo, G., Donato, R., and Di Stefano, F.: Gli habitat sottomarini delle coste della Campania, *Biologi Italiani*, 6,
687 2008.
- 688 Sacchi, M., Insinga, D., Milia, A., Molisso, F., Raspini, A., Torrente, M. M., and Conforti, A.: Stratigraphic
689 signature of the Vesuvius 79 AD event off the Sarno prodelta system, Naples Bay, *Marine Geology*, 222–223, 443–
690 469, <https://doi.org/10.1016/j.margeo.2005.06.014>, 2005.
- 691 Sacchi, M., Molisso, F., Violante, C., Esposito, E., Insinga, D. D., Lubritto, C., Porfido, S., and Toth, T.: Insight
692 into flood dominated, mixed slioclastic-volcanoclastic fan deltas: very high-resolution seismic examples off the
693 Amalfi cliffed coast, Eastern Tyrrhenian Sea, in: *Geohazard in rocky coastal areas*, edited by: Violante, C.,
694 Geological Society, London, UK, 32–71, 2009.

Codice campo modificato

695 Sacchi, M., Pepe, F., Corradino, M., Insinga, D.D., Molisso, F., Lubritto, C.: The Neapolitan Yellow Tuff caldera
696 offshore the Campi Flegrei: Stratal architecture and kinematic reconstruction during the last 15ky, *Marine Geology*,
697 354, 15-33, 2014

698 Sacchi, M., Caccavale, M., Corradino, M., Esposito, G., Ferranti, L., Hámori, Z., † F., Insinga, D., Marino, C.,
699 Matano, F., Molisso, F., Natale, J., Passaro, S., Pepe, F., and Toth, T.: The use and beauty of ultra-high-resolution
700 seismic reflection imaging in Late Quaternary marine volcanoclastic settings, Napoli Bay, Italy, *Földtani Közöny*,
701 149, 371, <https://doi.org/10.23928/foldt.kozl.2019.149.4.371>, 2019.

702 [Sappington, J. M., Longshore, K. M., and Thompson, D. B.: Quantifying Landscape Ruggedness for Animal](#)
703 [Habitat Analysis: A Case Study Using Bighorn Sheep in the Mojave Desert, *The Journal of Wildlife Management*,](#)
704 [71, 1419–1426, <https://doi.org/10.2193/2005-723>, 2007.](#)

705 Sievers, J., Milbradt, P., Ihde, R., Valerius, J., Hagen, R., and Plüß, A.: An integrated marine data collection for
706 the German Bight – Part 1: Subaqueous geomorphology and surface sedimentology (1996–2016), *Earth System*
707 *Science Data*, 13, 4053–4065, <https://doi.org/10.5194/essd-13-4053-2021>, 2021.

708 Slooman, A., & Cartigny, M. J.: Cyclic steps: review and aggradation-based classification. *Earth-Science Reviews*,
709 201, 102949, 2020.

710 Somma, R., Iuliano, S., Matano, F., Molisso, F., Passaro, S., Sacchi, M., Troise, C., De Natale, G.: High - resolution
711 morpho-bathymetry of Pozzuoli Bay, southern Italy, *Journal of Maps*, 12(2), 222-230, 2016.

712 Stall, S., Yarmey, L., Cletcher-Gershenfeld, J., Hanson, B., Lehnert, K., Nosek, B., Parsons, M., Robinson, E., and
713 Wyborn, L.: Make scientific data FAIR, *Nature*, 570, 27–29, <https://doi.org/10.1038/d41586-019-01720-7>, 2019.

714 Steinmann, L., Spiess, V., Sacchi, M.: The Campi Flegrei caldera (Italy): Formation and evolution in interplay with
715 sea-level variations since the Campanian Ignimbrite eruption at 39 ka. *Journal of Volcanology and Geothermal*
716 *Research* 327, 361-374, 2016.

717 Tanhua, T., Hainbucher, D., Cardin, V., Álvarez, M., Civitarese, G., McNichol, A. P., and Key, R. M.: Repeat
718 hydrography in the Mediterranean Sea, data from the *Meteor* cruise 84/3 in 2011, *Earth System Science Data*, 5,
719 289–294, <https://doi.org/10.5194/essd-5-289-2013>, 2013.

720 Taviani, M., Angeletti, L., Cardone, F., Montagna, P., and Danovaro, R.: A unique and threatened deep water coral-
721 bivalve biotope new to the Mediterranean Sea offshore the Naples megalopolis, *Sci Rep*, 9, 3411,
722 <https://doi.org/10.1038/s41598-019-39655-8>, 2019.

723 Trincardi, F., and Zitellini, N.: The rifting of the Tyrrhenian basin. *Geo-Marine Letters*, 7, 1-6,
724 <https://doi.10.1007/BF02310459>, 1987.

725 Trincardi, F., Francocci, F., Pellegrini, C., Ribera d'Alcalà, M., and Sprovieri, M.: Chapter 13 - The Mediterranean
726 Sea in the Anthropocene, in: *Oceanography of the Mediterranean Sea*, edited by: Schroeder, K. and Chiggiato, J.,
727 Elsevier, 501–553, <https://doi.org/10.1016/B978-0-12-823692-5.00013-3>, 2023.

728 Violante, C., Budillon, F., Esposito, E., Porfido, s., Vittori, E.: Submerged hummocky topographies and relations
729 with landslides, northwestern flank of Ischia Island, southern Italy, in: *Proceedings of the International Workshop*

ha formattato: Inglese (Stati Uniti)

730 on Occurrence and mechanisms of flow-like landslides in natural slopes and earthfills, Sorrento, Italy, May 2003,
731 14-16, 2003.

732 Walbridge, S., Slocum, N., Pobuda, M., and Wright, D.: Unified Geomorphological Analysis Workflows with
733 Benthic Terrain Modeler, *Geosciences*, 8, 94, <https://doi.org/10.3390/geosciences8030094>, 2018.

734 Weiss, A. D.: Topographic positions and landforms analysis, Poster Presentation, ESRI User Conference, San
735 Diego, CA, 2001.

736 Worm, B., Barbier, E. B., Beaumont, N., Duffy, J. E., Folke, C., Halpern, B. S., Jackson, J. B. C., Lotze, H. K.,
737 Micheli, F., Palumbi, S. R., Sala, E., Selkoe, K. A., Stachowicz, J. J., and Watson, R.: Impacts of Biodiversity Loss
738 on Ocean Ecosystem Services, *Science*, 314, 787–790, <https://doi.org/10.1126/science.1132294>, 2006.

739